

RDB FOR RETENTION  
OR DESTRUCTION ✓

TR-108

R. Rastby



## TECHNICAL REPORT

# SUBMARINE GEOLOGY OF THE TONGUE OF THE OCEAN, BAHAMAS

NOVEMBER 1962

(Reprinted 1968)



NAVAL OCEANOGRAPHIC OFFICE  
WASHINGTON, D. C. 20390

Price \$1.20

GC  
1

.T43

no. TR-108

## A B S T R A C T

Seventy-three sediment cores, 6 grab samples, and 4 stereographic camera tracks were taken on the bottom and flanks of the Tongue of the Ocean, Bahamas. The Tongue of the Ocean is a long, deep re-entrant or channel into the Great Bahama Bank. It is oriented northwest-southeast, is about 700 fathoms deep in its southern portion (cul-de-sac), and gradually descends northward to 1,300 fathoms over a distance exceeding 100 miles. The flanks or walls of the channel are precipitous and average  $15^{\circ}$  to  $20^{\circ}$  slope above 250 to 300 fathoms depth; however, the slope below this depth range to the bottom is more gradual. Incised into the flanks are deep gullies trending at right angles to the surrounding bank edges; the gullies are more prevalent in the long, narrow northern portion of the channel than in the southern cul-de-sac area.

Laboratory analyses show the bottom sediment to be predominantly silt-sized skeletal and nonskeletal carbonate particles of both deep and shallow water origin. Organic carbon content of the sediment is low, averaging between 1.0 and 2.0 percent. Water content, void ratio, and porosity decrease with depth in the sediment, while conversely, density and cohesion increase.

Sediment accumulation in the channel can be attributed to slow, continuous particle-by-particle deposition from the overlying water column and turbidity current type deposition originating on the upper walls and bank edges of the channel. The latter type accumulation accounts for over 50 percent of the sediment column sampled. Rate of sediment accumulation is extremely high along the flanks and central reaches of the southern portion in the channel. Radiological dating shows accumulation as high as 640 cm/1,000 years at selected areas. Sediment accumulation in the northern, central area of the Tongue of the Ocean is much less and is measured at between 3 to 5 cm/1,000 years.

Stereographic photographs of the channel bottom show a paucity of benthic animal or plant life, and, in general, an almost featureless unconsolidated ooze is pictured. In the central, northern portion of the channel at 1,000- fathoms depth, a limestone outcrop is present containing cavities or basins suggestive of subaerial erosion at some earlier geologic time. Adjacent to the outcrop are well-developed symmetrical ripple marks probably caused by tidal oscillations or internal waves, and, on the basis of ripple form and dominant sediment grain size, bottom currents of between 0.3 to 1.0 knot are calculated.

ROSWELL F. BUSBY


*Oceanographic Development Division*

## FOREWORD

This report brings up-to-date all the information and observations collected by this Office concerning the submarine geology of the Tongue of the Ocean, Bahamas. Reports and work of other agencies and individuals have been used where necessary in the preparation of this Technical Report.

Research work on the submarine geology of the Tongue of the Ocean is continuing, but the major concentration now is on the shallow banks surrounding the channel.

It is believed that the analyses contained in this report will contribute significantly toward the understanding of the complex marine environment found in the Tongue of the Ocean area.

  
E. C. STEPHAN  
Rear Admiral, U. S. Navy  
Commander





## PREFACE

The investigations of the submarine geology of the Tongue of the Ocean reported herein were begun in 1961. The author, Roswell F. Busby, has been active in collecting the data as well as in performing the laboratory analyses and interpreting the results.

The author would like to acknowledge the following personnel from the Oceanographic Office: W. E. Maloney for providing support and permission to pursue the investigations, G. H. Keller for performing the bulk of the engineering tests and for offering suggestions in the preparation of the report, and B. K. Swanson for critically reviewing the manuscript.

The author would also like to express gratitude to the Marine Laboratory, University of Miami, for use of their laboratory facilities, and to Dr. Gene A. Rusnak for making available information and figures in advance of a forthcoming paper and for his many helpful suggestions and encouragement in the preparation of this report.

Finally, appreciation is extended to Commander R. L. Sattler and the officers and enlisted men of the USS SAN PABLO (AGS-30) for providing the means and assistance in collecting the samples and observations used in the report.



# TABLE OF CONTENTS

	Page
FOREWORD . . . . .	iii
PREFACE . . . . .	v
FIGURES . . . . .	viii
TABLES . . . . .	viii
PLATES . . . . .	ix
APPENDIX . . . . .	ix
INTRODUCTION . . . . .	1
Purpose of the Investigation . . . . .	1
Description of the Area . . . . .	1
REVIEW OF PERTINENT LITERATURE . . . . .	6
The Bahama Platform . . . . .	6
The Tongue of the Ocean . . . . .	7
PRESENT INVESTIGATION . . . . .	9
Field Procedure . . . . .	9
Laboratory Analyses . . . . .	9
SEDIMENTS . . . . .	13
General . . . . .	13
Near-flank Sediments . . . . .	15
Axial Sediments . . . . .	25
Cul-de-sac Sediments . . . . .	33
RATE OF SEDIMENT ACCUMULATION . . . . .	45
ENGINEERING PROPERTIES . . . . .	48
Shear Strength . . . . .	48
Sensitivity . . . . .	57
BOTTOM PHOTOGRAPHY . . . . .	58
Camera Station Data . . . . .	58
Biology . . . . .	60
Bottom Features . . . . .	61
Bottom Currents . . . . .	62
SUMMARY . . . . .	64
REFERENCES CITED . . . . .	66

## FIGURES

	Page
1 Bahama Platform . . . . .	2
2 Bathymetry of the TOTO (after Athern, 1962 a) (fold-in) . . . . .	3
3 Longitudinal and Cross Sectional Profiles of the TOTO . . . . .	5
4 Sediment Sampling Stations in the TOTO . . . . .	10
5 Location of Deep-sea Camera Lowerings and Vertical Profiles . . . . .	11
6 Areal Distribution of Sediment Types in the TOTO . . . . .	14
7 Longitudinal Cross Section of Near-flank Cores (fold-in) . . . . .	17
8 Longitudinal Cross Section of Axial Cores (fold-in) . . . . .	27
9 Longitudinal Cross Section of Cul-de-sac Cores (fold-in) . . . . .	39
10 Rate of Bulk Sediment Accumulation at Selected Locations in the TOTO . . . . .	46
11 Frequency of Turbidity Current Flows at Various Locations in the TOTO . . . . .	47
12 Areas of High (>1.0 psi) and Low Cohesion in the TOTO . . . . .	50
13 Distribution of Surface Sediment Organic Carbon Content (%) . . . . .	51
14 Plots of Ship's Position During Camera Lowerings . . . . .	59

## TABLES

I Particle size analyses of near-flank sediments . . . . .	19
II Near-flank sediment density, water content, void ratio, and porosity . . . . .	22
III Particle size analyses of axial sediments . . . . .	29
IV Axial sediment density, water content, void ratio, and porosity . . . . .	34
V Particle size analyses of cul-de-sac sediments . . . . .	41
VI Cul-de-sac sediment density, water content, void ratio, and porosity . . . . .	43
VII Shear strength and sensitivity of the TOTO sediments . . . . .	52



## PLATES

	Page
I AXIAL CORE 62-16 (TOP) AND NEAR-FLANK CORE 62-15 (BOTTOM) . . . . .	71
II TURBIDITE ZONE IN CORE 62-48B . . . . .	72
III REPRESENTATIVE BOTTOM PHOTOGRAPHS FROM CAMERA STATION 1 . . . . .	73
IV BOTTOM PHOTOGRAPHS FROM CAMERA STATION 1 . . . . .	74
V REPRESENTATIVE BOTTOM PHOTOGRAPHS FROM CAMERA STATION 2 . . . . .	75
VI REPRESENTATIVE BOTTOM PHOTOGRAPHS FROM CAMERA STATION 3 . . . . .	76
VII REPRESENTATIVE BOTTOM PHOTOGRAPHS FROM CAMERA STATION 4 . . . . .	77
VIII MOSAIC OF THE OUTCROP AS PHOTOGRAPHED BY THE CAMERA SYSTEM . . . . .	78
IX CAVITIES AND DEPRESSIONS AT 1,000 FATHOMS IN THE TONGUE OF THE OCEAN . . . . .	79
X MICROTOPOGRAPHIC CONTOUR MAP OF PLATE IX . . . . .	80
XI BOTTOM PHOTOGRAPHS FROM CAMERA STATION 4 . . . . .	81

## APPENDIX

I CORE STATION DATA . . . . .	83
-------------------------------	----

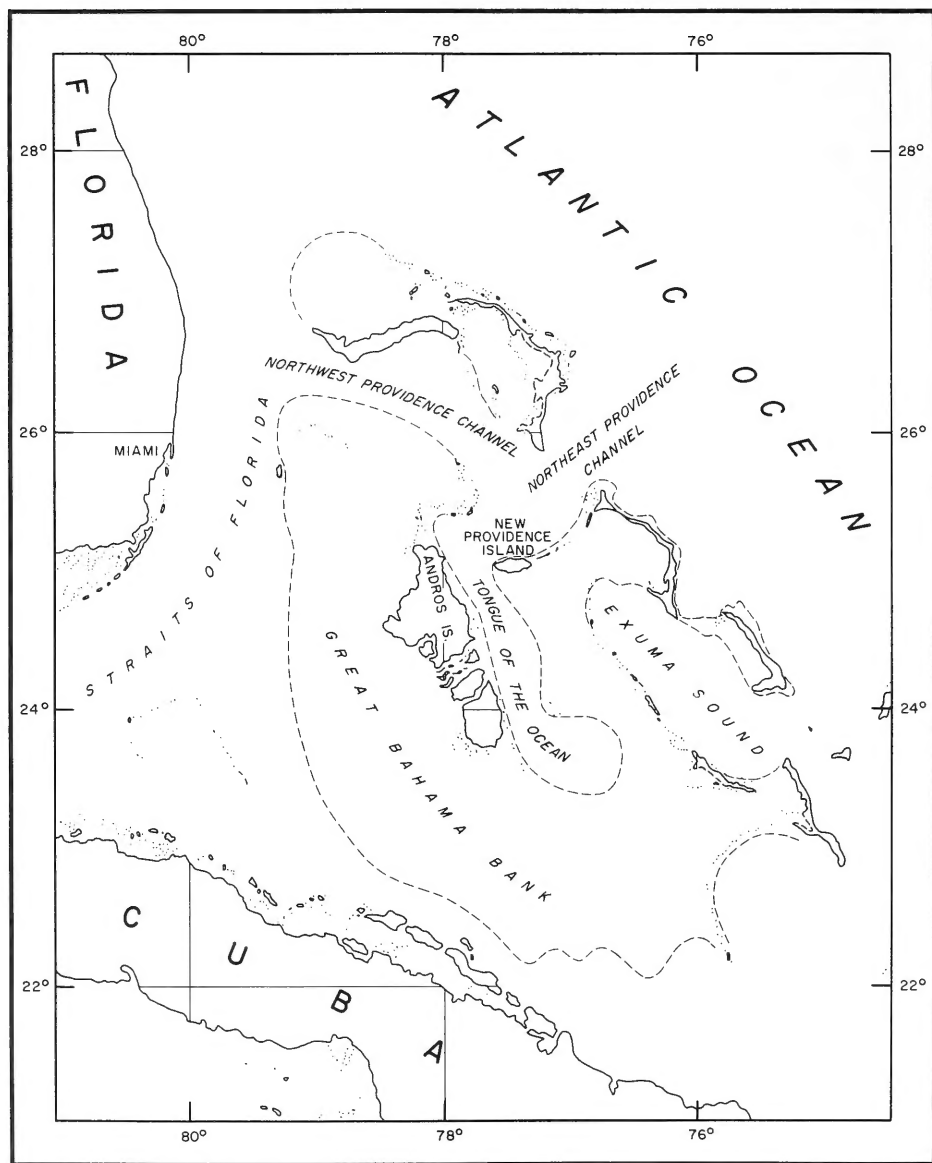


FIGURE 1 THE BAHAMA PLATFORM

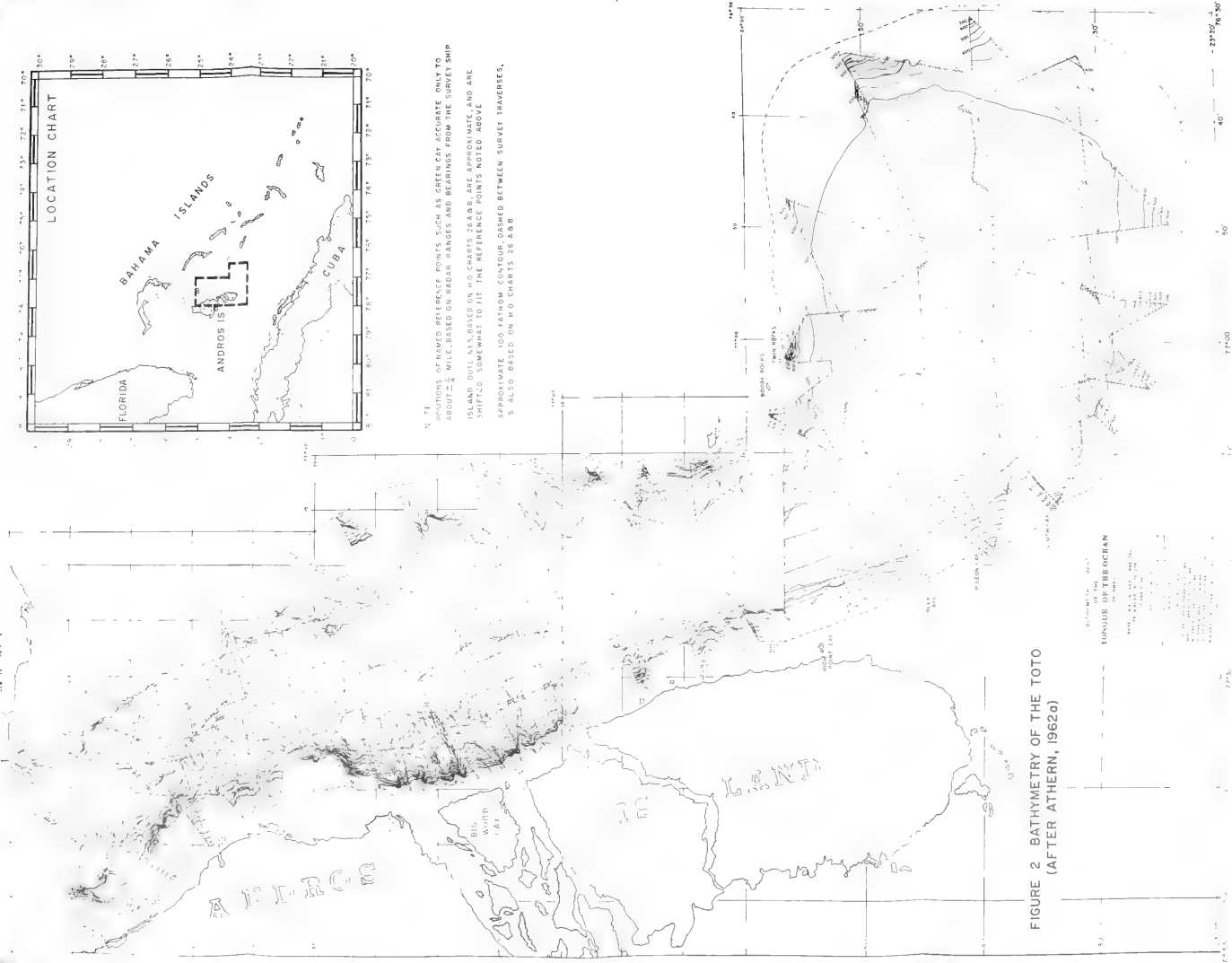


FIGURE 2 BATHYMETRY OF THE TOTO  
(AFTER ATHERN, 19620)



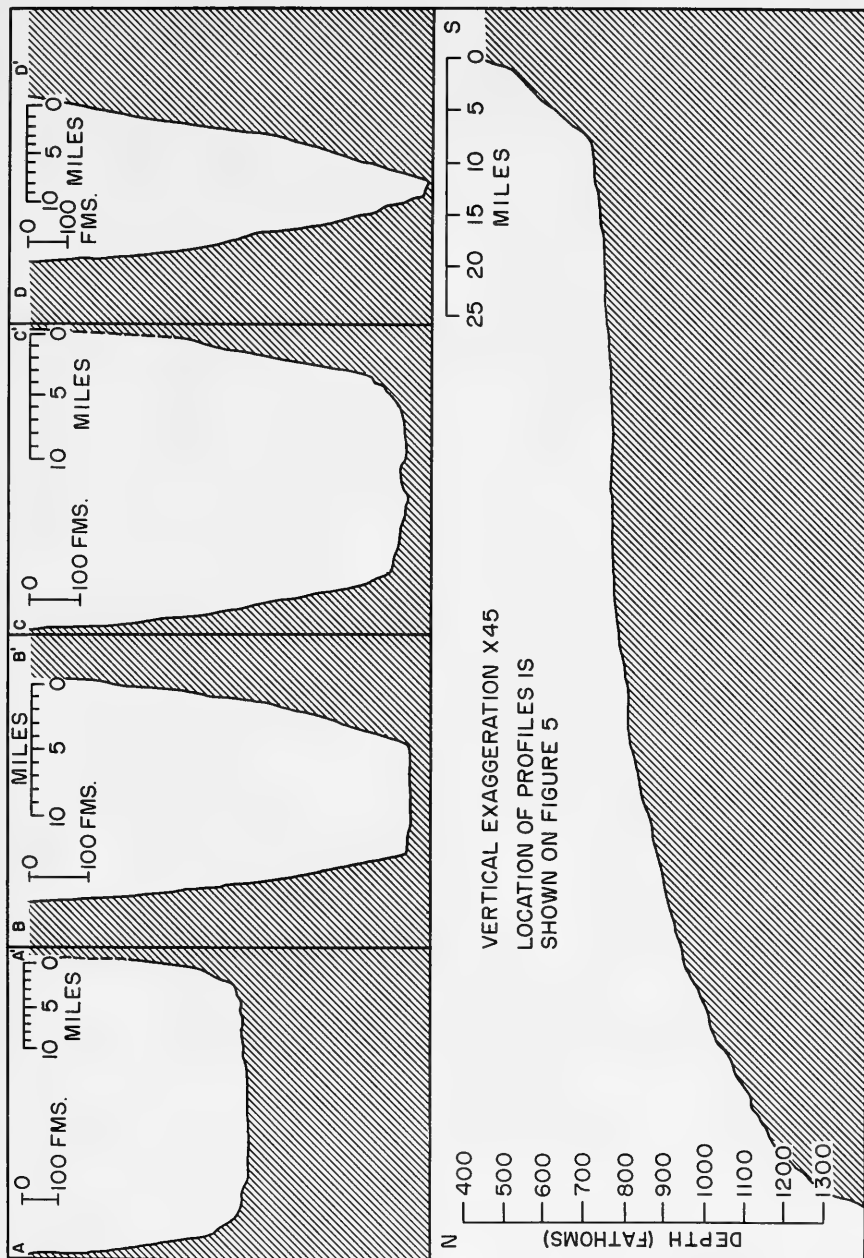


FIGURE 3 LONGITUDINAL AND CROSS SECTIONAL PROFILES OF THE TOTO

## REVIEW OF PERTINENT LITERATURE

### The Bahama Platform

The Bahama Platform (or Bahama Block), representing, as it does, a contemporary example of warm, shallow limestone seas such as occurred during earlier geological times, has been the object of investigation by many students of carbonate geology. However, the majority of investigations have been concentrated on the sedimentary material covering the shallow banks, and until recently there was scant information dealing with sediments in the deep channels.

Some of the more extensive contributions to the literature of Bahamian shallow-water sediments were made by Agassiz (1894), Vaughan (1913, 1914, and 1918), Drew (1914), Goldman (1926), Field (1931), Thorp (1936), Newell et al (1951), Newell and Rigby (1957), and Illing (1954). These studies dealt primarily with the grains comprising the deposits, their origin, composition, and general distribution throughout selected areas on the bank, as well as reports on various land forms, reef corals, and topographic features present on the surface and flanks of the Platform.

Mode of origin and internal structure of the Bahama Banks has received the attention of various individuals. One of the first to speculate on the genesis of this structure was Nelson (in Schuchert, 1935), who entertained the view that the Bahamas were essentially of deltaic origin, and that the materials composing the Banks were derived from the waters of the Gulf Stream which were checked by Atlantic waters as the Gulf Stream emerged full strength from the Gulf of Mexico. Woodring (1928) believed that the Bahamas represented a series of West Indian Cretaceous folds that were worn down and submerged; the highest points subsequently being covered with a veneer of calcareous sand.

Field (1931), on the basis of gravity data and stratigraphic observations on various Bahamian Islands, stated that the Bahamas are not underlain by igneous rock and probably did not originate as the result of volcanic action. He concluded that although the Block is approximately in isostatic equilibrium it appears to be somewhat unstable, having undergone several slight vertical movements. Hess (1933), utilizing gravity and bathymetric data, showed that a great submergence in excess of 14,000 feet has taken place in the Bahamas, and the general field of negative anomalies he observed over the Bahama Block is due to a vast thickness of light sediment beneath the Bahamas; however, the dolomitic reef material being relatively heavy causes the anomalies on the reef to be less negative than those in the deep channels. Schuchert (1935) held that the northern Bahama Banks and the western portion of the Great Bahama Bank were composed of essentially unfolded sedimentary strata belonging to the Mexico-Florida foreland plate, while the eastern half of the Great Bahama Bank and the southeast trending archipelago were volcanic in origin and postdated the sedimentary portion of the Bahamas.

Spencer (in Eardley, 1951) cited an Andros Island deep boring (14,587 feet deep) which showed relatively pure, shallow-water carbonates of Tertiary and Cretaceous

age; the latter constituting about half of the entire sequence. Newell (1955) stated that the coarse, open cavernous texture found at many horizons in the above boring indicated leaching near sea level; thus, making the unavoidable conclusion that this part of the shelf had quietly subsided more than  $2\frac{1}{2}$  miles since early Cretaceous, and that it is still sinking while the Platforms are being built up near the surface by accumulation of calcium carbonate. He calculated an average rate of accumulation of consolidated sediment on the Great Bahama Bank of about 3.6 cm per 1,000 years.

Gravity data, interpreted by Worzel et al (1953), show a small seaward increase of gravity across the Platform, with negative free air anomalies of about 110 milligals along the eastern boundaries of the Bahamas and southern part of the Blake Plateau.

Evaluating all existing data, Newell (1955) concluded that the region has long been isolated from sources of terrigenous sediments, that no compelling evidence exists of folding or faulting in later geologic times, and that little data have been presented to show that frequent interruptions in the general subsidence (probably the result of isostatic adjustment to the steady accumulation of carbonates) have occurred during the past 130 million years or so.

### The Tongue of the Ocean

The majority of reports on the TOTO have been primarily concerned with the method of channel formation and are based on gravity, bathymetric, and seismic data. However, recently a number of sediment samples have been collected from the floor of the TOTO which give a somewhat general picture of the material covering the bottom and the mode of deposition.

Origin: Hess (1933) attributed initial formation of the deep Bahamian channels to the action of running water under subaerial conditions; the drainage patterns being structurally controlled by some unknown factors. Subsequent to formation of the erosional valleys, subsidence and rapid deposition of calcareous material on the higher prominences formed the present Bahamian platforms and channels. Hess (Ibid.) further stated that the continuous slope of the valley floors from the upper reaches of the channels to the edge of the continental slope excluded a graben and synclinal-trough hypothesis, and noted that marine erosion is not likely to produce a valley with an inner gorge or channel running down the middle and a continuous slope in one direction.

Schuchert (1935) advanced the hypothesis that Andros Island once faced the open Atlantic, and later the suspected volcanic eastern portion of the Great Bahama Bank grew up in front of Andros leaving the Tongue of the Ocean between.

Ericson et al (1952), on the basis of lithological and paleontological evidence from sediment cores collected in the TOTO, concluded that turbidity current erosion may be largely responsible for excavation of the TOTO and Providence Channels.

Worzel et al (1953) re-examined gravity observations collected from the Banks, and, in reference to the origin of the TOTO, concluded that most of the anomalies can be explained by simple erosion of the deep-water portions without compensation, or, alternately, construction of the shallow-water portions without regional compensation. Newell (1955) combined both of these alternatives and theorized that the

deep channels are mainly the result of constructional processes through differential deposition and bypassing.

On the other hand, Talwani and Worzel (in Siegler, 1961) collected additional gravity data and attributed negative residual anomalies of -30 to -40 milligals over the deeply incised portions of the Bank to faulting which resulted in the heavier sediment occurring at greater depths.

A technical report by the University of Miami (1958) stated that lack of a source of large quantities of sediment negates the possibility of turbidity current erosion creating the TOTO, but, suggested that the channel originated through some type of block faulting.

Bottom Sediments: The first reported bottom samples taken from the TOTO were collected by Vaughan (1918). He classified the sediment as globigerina ooze, and also performed size and mineralogical analyses on the two cores collected. Armstrong (1953) collected dredge and core samples from the TOTO and bottom photographs at selected locations. The photographs show an almost vertical bare rock wall down to 230 meters, and at 383 meters sand and gravel covers the rock. Between 500 and 600 meters depth the sands and gravels are intermixed and finally replaced by calcareous mud which becomes increasingly finer with depth to the bottom of the channel (2,200 meters in the area examined).

Analyses of cores and dredge samples taken from the TOTO are presented in a technical report by the University of Miami (1958). This report classified the bottom material as globigerina, pteropod, and oolitic ooze. The report also presented the results of sediment size, moisture, faunal, and semiquantitative spectrographic analyses. The report discussed the hummock-like appearance of the slope along the entire length of the TOTO between 300 and 550 fathoms. This feature was considered to be talus that probably originated from stirring up of material found on the top of the bank in addition to turbidity currents originating on the edge of the bank which augmented the talus slope.

Ostlund et al (1962) presented the results of radiocarbon measurements of the TOTO sediment cores collected by the Marine Laboratory, University of Miami, and discussed the age of the sediment, bulk rate of accumulation, and frequency of turbidity current flows in various areas of the channel.

Athern (1962 a & b) undertook a detailed bathymetric reconnaissance of the TOTO, collected sediment cores from the central flat reaches of the channels, and obtained 78 bottom photographs at various locations.

Rusnak and Nesteroff (1962) discussed the structural characteristics of turbidity current deposits in the TOTO, their composition, area of origin, and frequency of occurrence. They further compared the characteristics of turbidity current deposits in the TOTO to abyssal plain terrigenous deposits laid down in a similar manner.



## PRESENT INVESTIGATION

### Field Procedure

Seventy-three sediment cores, 6 grab samples, and 4 deep sea camera lowerings were made from aboard USS SAN PABLO (AGS-30) during September 1961 and February 1962. The cores were collected at depths varying from 430 to 2,800 meters, and the average length of each core collected was 99 centimeters. Fifteen of the sediment samples were obtained with a Hydro-plastic piston corer and the remainder with a Kullenberg gravity corer. Cores obtained with the Kullenberg apparatus were coated with a microcrystalline wax a few hours after collection to inhibit loss of moisture. In a few instances the hydrogen ion (pH) concentration at the top of the core was measured with a Beckman pH meter. A small portion from the top and bottom of each core was removed as soon as the core was brought aboard and stored under refrigeration while awaiting organic carbon analyses.

Sampling stations were positioned by Decca Hi-Fix navigational aids in the area of the TOTO north of Green Cay, and visual and radar fixes were used in the cul-de-sac. Locations of sampling stations are presented in Figure 4, and coordinates of sampling station, length of core, and water depth are listed in Appendix I.

Photographs of the bottom were taken with an underwater camera system consisting of two 35 mm cameras and two 100 watt-seconds strobe light sources. A sonar pinger, mounted on the camera frame and used in conjunction with the ship's transducer, and a Precision Graphic Recorder provided monitoring of the camera-to-bottom distance. A compass direction vane was suspended below the cameras to indicate direction of camera movement and orientation of the photographs.

The camera system was held within 5 feet of the desired 15 feet from the bottom distance during the photographing sequence. Between 276 and 572 meters was traversed during the 2-hour period of each lowering. Along these tracks, photographs of the bottom were taken every 14 seconds. Subsequent to the field operations, relief from selected photographs was measured and contoured. Camera lowering positions are shown on Figure 5.

### Laboratory Analyses

Utilizing facilities provided by the Marine Laboratory, University of Miami, all cores were analyzed within two weeks from the date of collection. Subsequent to lithological examination and engineering properties analyses, subsamples from the cores were forwarded to the Oceanographic Office for further analyses. The following is a tabulation of the analyses performed and description of the terms employed in the data summation tables and the text:

Constituents: A visual estimate, based on microscopic examination, of the constituents constituting the sand size and larger material present in selected core subsamples.

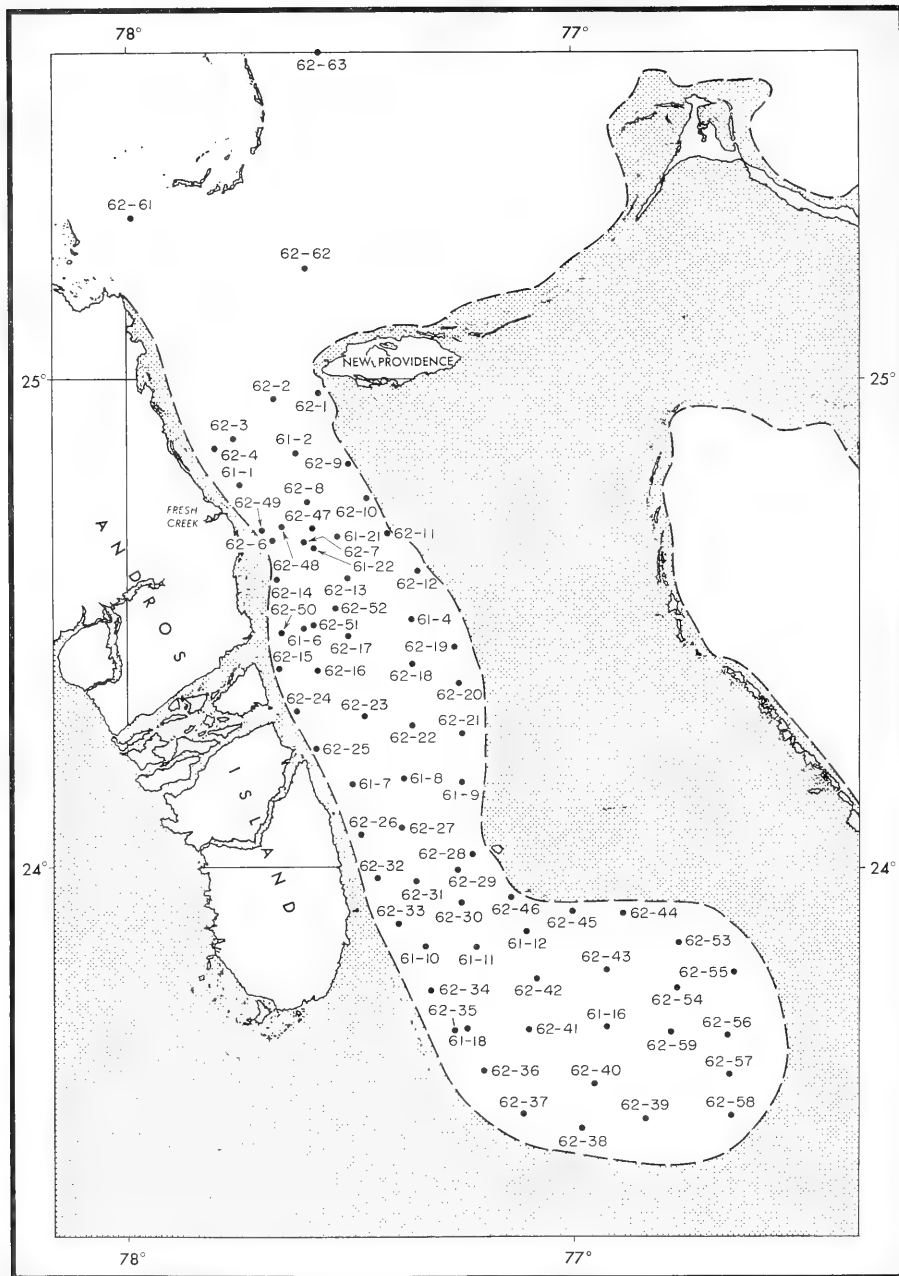


FIGURE 4 SEDIMENT SAMPLING STATIONS IN THE TOTO

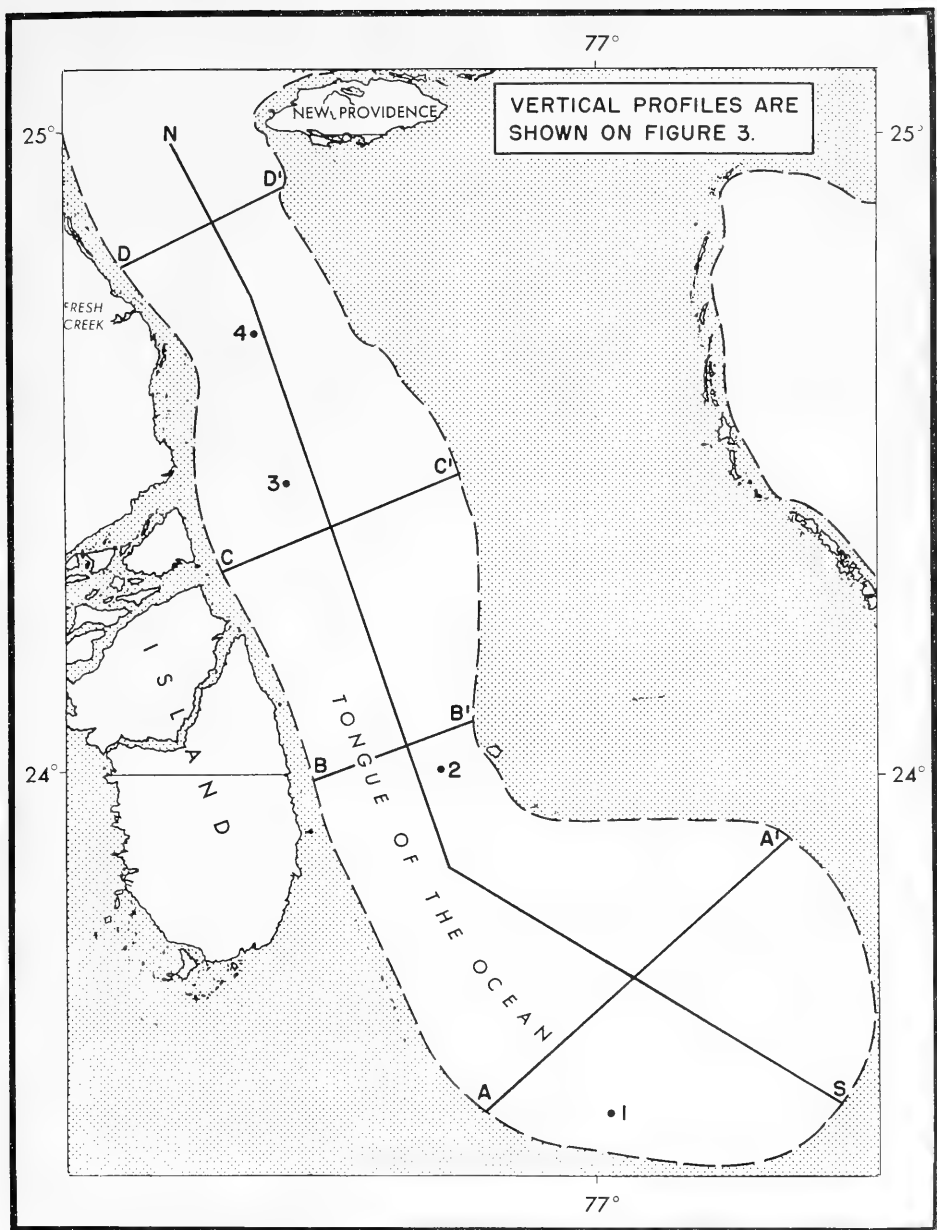


FIGURE 5 LOCATION OF DEEP-SEA CAMERA LOWERINGS AND VERTICAL PROFILES

Calcium Carbonate (%): A determination of the total alkaline earths through titration with EDTA as described by Turkian (1956). The method assumes that the amount of magnesium and strontium carbonates in the samples is trivial, and results are reported as calcium carbonate ( $\text{CaCO}_3$ ) solely.

Organic Carbon (%): The organic carbon present in the sediment as determined by the potassium dichromate ferrous ammonium sulfate titration method of Allison (1935).

Specific Gravity of Solids: The ratio of the sediment sample weight in air to its weight in water at  $4^\circ\text{C}$ .

Cohesion ( $\text{lbs}/\text{in}^2$ ): The shear strength as measured by standard soil mechanic techniques utilizing vane shear and compression testing apparatus. The procedure, significance, and reliability of this measurement as employed by the Oceanographic Office is discussed by Richards (1961).

Sensitivity: The ratio of the undisturbed strength of the sediment to disturbed strength at an unaltered water content.

#### SENSITIVITY SCALE (after Richards, 1961)

Sensitivity	Description	Percentage of "Undisturbed" Strength Lost in Remolded State
< - 1	Insensitive	0
1 - 2	Slightly insensitive	0 to 50.0
2 - 4	Medium sensitive	50.0 to 75.0
4 - 8	Very sensitive	75.0 to 87.5
8 - 16	Slightly quick	87.5 to 93.8
16 - 32	Medium quick	93.8 to 96.9
32 - 64	Very quick	96.9 to 98.4
> 64	Extra quick	> 98.4

Wet Unit Weight ( $\text{gm}/\text{cc}$ ): The bulk density of the sediment measured to the nearest tenth by means of wet weight per known volume of sediment.

Water Content (%): Ratio in percent of the weight of water to the weight of the dried solid particles in a given sediment mass.

Void Ratio ( $e$ ): The ratio between the volume of voids ( $V_v$ ) and the volume of solids ( $V_s$ ).

$$e = \frac{V_v}{V_s}$$

Color: Color of sediment is based on the Geological Society of America Rock-Color Chart.

Sediment Grain Size: The sediment grain size scale used is the one categorized by the classification set forth in the Wentworth grade scale (Wentworth, 1922) with one modification. The term clay has been replaced by the term lutite because of the mineralogical implications of the former. The range of grade size in millimeters diameter and phi units [ $0 = -\log_2$  diameter (millimeters)] is shown below:

	Particle Diameter (mm)	Particle Diameter (phi)
Granules	2.0000 to 4.0000	-2 to -1
Coarse sand	0.5000 to 2.0000	-1 to 1
Medium sand	0.2500 to 0.5000	1 to 2
Fine sand	0.0625 to 0.2500	2 to 4
Silt	0.0039 to 0.0625	4 to 8
Lutite	< 0.0039	> 8

## SEDIMENTS

### General

On the basis of lithology and physical properties, the sediments collected from the TOTO are divided into 3 geographic categories; 1) near flank, 2) axial, and 3) cul-de-sac (Fig 6). The bottom sediments in the TOTO display properties and relationships distinctive of these areas in the channel, but, gradational transitions from one type sediment to the other is present, and combinations of various types exist.

Irrespective of lithological and physical variations in the sediments, both calcium carbonate content and specific gravity of the solids show no significant variation with depth or location, but are generally uniform throughout the bottom and vary between narrow margins. Of a total of 315 core subsamples analyzed for calcium carbonate, the maximum value obtained was 100 percent, the minimum 82 percent, and the average 94 percent. Specific gravity determinations were run on 32 subsamples from representative cores, and the values obtained ranged from 2.68 to 2.86 with an average of 2.79.

The results of a semiquantitative spectrochemical analysis by the University of Miami (1958) are given below, and may be taken to represent ( $\pm 20$  percent) other possible elements and compounds present in the TOTO sediments where  $\text{CaCO}_3$  does not comprise the entire sample.

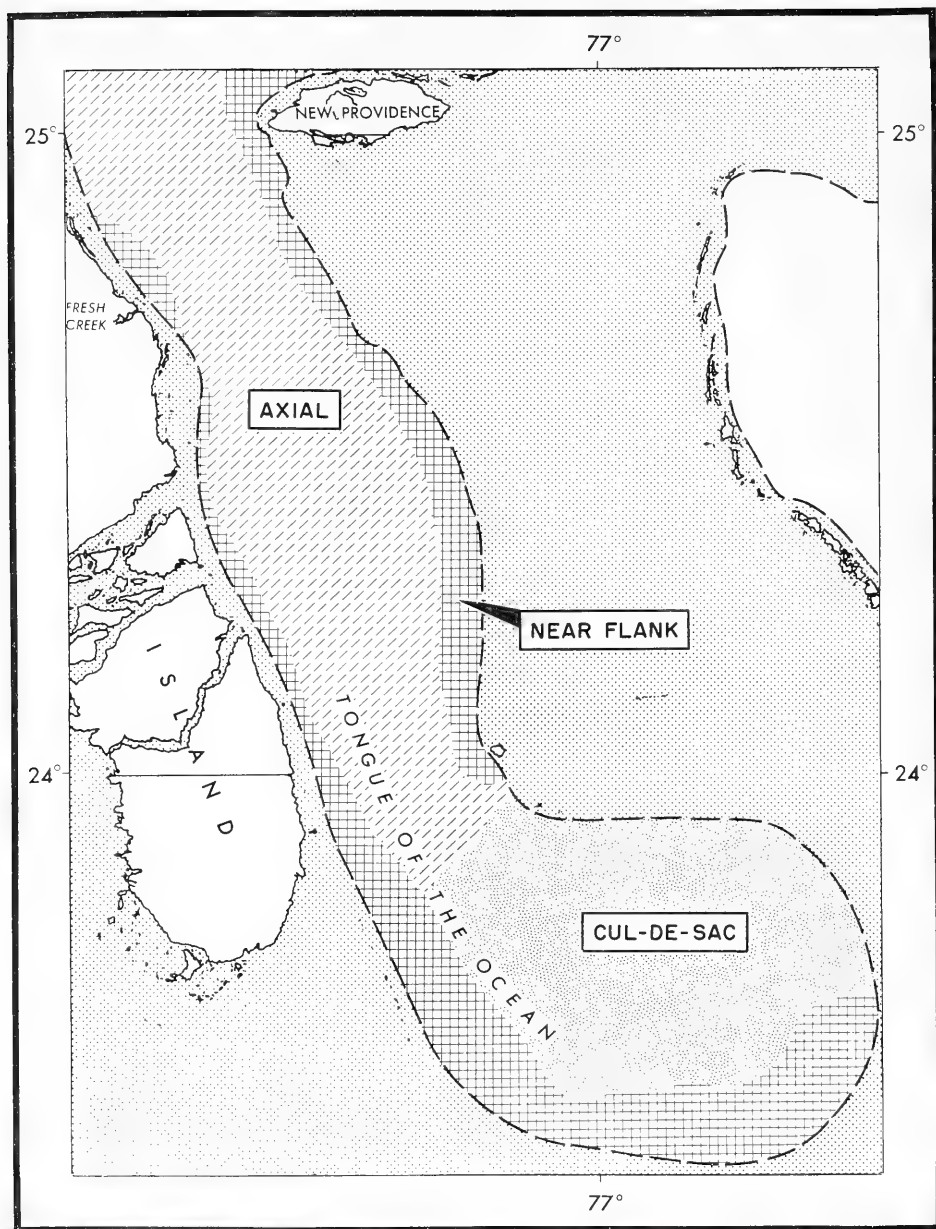


FIGURE 6 AREAL DISTRIBUTION OF SEDIMENT TYPES IN THE TOTO

Material	Amount (%)
CaCO <sub>3</sub>	85.000
SiO <sub>2</sub>	7.000
Al <sub>2</sub> O <sub>3</sub>	3.000
Na	2.000
Fe <sub>2</sub> O <sub>3</sub>	0.600
MgO	0.300
Ti	0.005
K	Trace
Sr	Trace
V	Trace
Zn	Trace

Except for the CaCO<sub>3</sub> content and the specific gravity which tend to remain constant in the sediments, other properties show a variation in magnitude which is generally dependent upon the area from which the sediment sample was obtained. These variations will be discussed below under the appropriate sedimentary category.

#### Near-flank Sediments

Sediments of the near-flank category are represented by the following samples:

62-1	62-23	62-37
62-4	62-24	62-38
62-6	62-25	62-39
62-9	62-26	62-57
62-10	62-28	62-58
62-14	62-32	61-1
62-15	62-33	61-9
62-19	62-34	61-10
62-20	62-35	61-18
62-21	62-36	

An examination of Figure 4 shows that these samples are all located on the flanks or walls bounding the TOTO and were collected from water depths between 250 and 1,243 meters.

Sediment color in the near-flank area is decidedly darker compared to other areas in the TOTO and is dominantly yellowish gray (5Y7/2) grading to a lighter greenish gray (5GY8/1). (Geological Society of America Rock-Color Chart code). The most striking property exhibited by these cores, except for a few from the southern flank of the cul-de-sac, is the smooth, even color and texture with depth in the sediment. Figure 7 presents a longitudinal cross section of selected near-flank cores, and, from this, the general homogeneity of particle grain size and sediment color is evident.

Cores 62-37 and 62-57 show a very sharp break in color at various depths in the core. Core 62-37 changes abruptly from a yellowish gray clayey silt to a pure white clayey silt with no apparent change in grain size or constituents. The white area is underlain by material similar to that above it, and the pattern is repeated within a few centimeters depth. The white area is far more cohesive than the material above and below it.

Cores 62-36, 62-38, and 62-39 are similar in most respects to the normal near-flank sediments, except for one or two zones of relatively coarse particles intermixed and separated from each other by finer material. These zones do not resemble layers which might have originated through turbidity current deposition but appear more like the result of sand "falls"; however, reworking of the material by organisms may have destroyed the original bedding, although other evidence of such activity is lacking. Sample 62-6, a grab sample, consisted of very coarse reef detritus, apparently from the nearby Andros Island barrier reef, and displayed the coarsest grained material of any taken from the channel.

Particle Size: Table 1 gives quartiles, median diameter, quartile deviation ( $QD\phi$ ) and skewness ( $Skq\phi$ ) values of subsamples from cores and grab samples in the near-flank area. Some general relationships are given below:

$$\begin{aligned} Q1\phi \text{ and } Q3\phi &= \text{1st and 3rd quartiles, respectively,} \\ Md\phi &= \text{Median diameter,} \\ QD\phi &= \frac{1}{2} (Q3 - Q1), \text{ and} \\ Skq\phi &= \frac{1}{2} (Q1 - Q3 - 2Md). \end{aligned}$$

In all samples (except three) the median diameter is within the range of silts, and, as well be shown later, this is by far the predominant particle size of the bottom sediments throughout the channel. The average grain-size distribution of near-flank sediments is 14 percent sand, 61 percent silt, and 25 percent lutite.

The quartile deviation ( $QD\phi$ ) is a measure of the average spread of points around the median (sorting), and when perfect sorting is obtained  $QD\phi$  is equal to zero. The sorting values in Table 1 show an almost equal number of poorly-sorted and normally-sorted samples. This is in sharp contrast to Illing (1954), who found sorting values for the adjacent bank sediments to be so uniformly low that it was necessary to break down the well-sorted category into smaller increments in order for the values to be meaningful.

Quartile skewness ( $Skq\phi$ ) is a measure of the symmetry or asymmetry of the curve of particle-size distribution. If the curve is perfectly symmetrical, then  $Skq\phi$  is equal to zero. If the spread of particle size is greater on the fine side (positive values) of the median diameter, then  $Skq\phi$  is positive, or if greater on the coarse side, then the value is negative. The greater spread of particle sizes on the fine side of the median diameter in these sediments shows the dominance of fine material in the near-flank area and may be the result of sediment winnowing by waves and currents on the shallow banks adjacent to and above this area. Water movement on the bank may stir up the bottom material and allow the coarser grains to resettle while maintaining the finer debris in suspension. The fine material is then carried to the edge of the bank, and, due to a



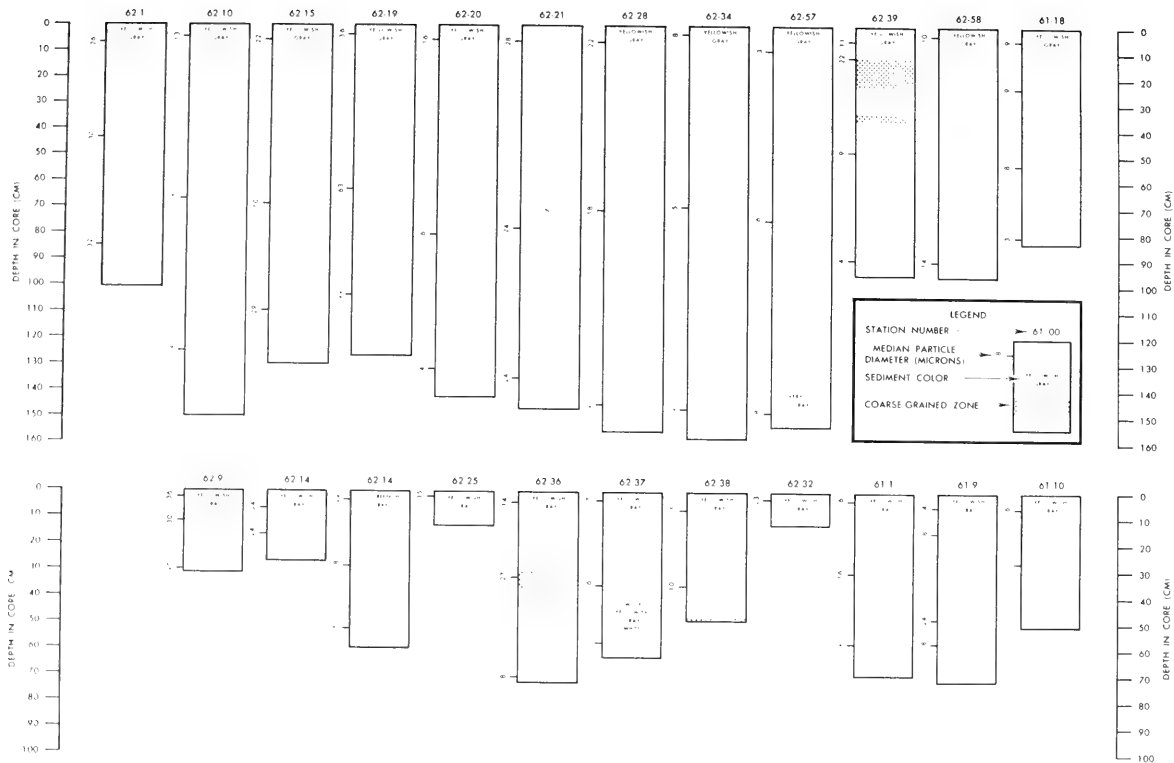
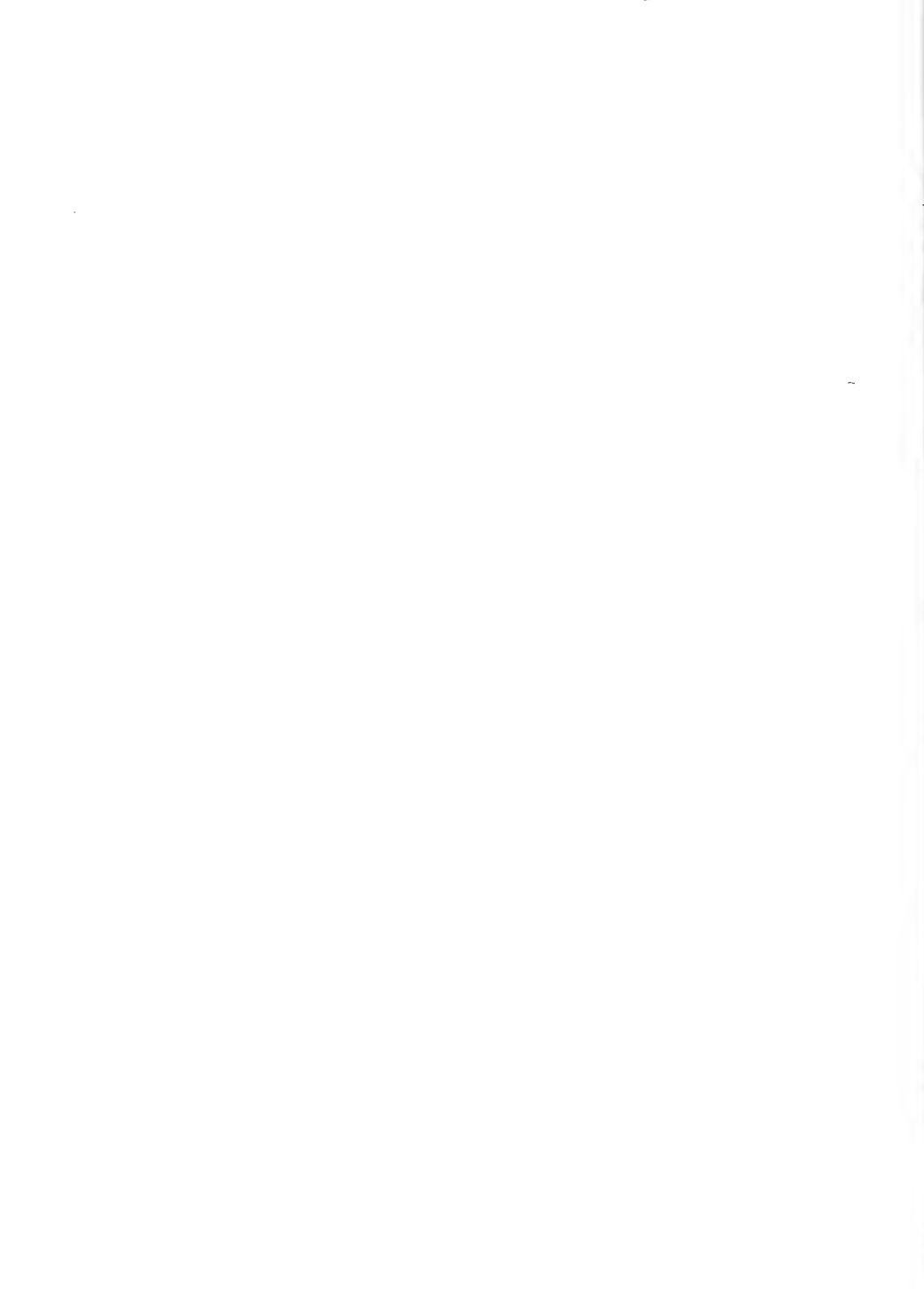


FIGURE 1. LONGITUDINAL CROSS SECTION OF NEAR-FLANK CORES



decrease in current velocity over the deep channel, the material settles through the water column and is deposited in the near-flank area.

TABLE I  
Particle size analyses of near-flank sediments

Core No.	Depth in Core (cm)	Q1 $\phi$	Md $\phi$	Q3 $\phi$	QD $\phi$	Skq $\phi$
62-1	8	4.16	5.29	7.03	1.44	0.31
	48	4.00	5.12	6.82	1.41	0.29
	94	4.24	5.49	7.57	1.67	0.42
62-4	Grab	4.16	5.01	5.86	0.85	-0.01
62-6	Grab	-3.84	-2.40	-0.93		
62-9	2	3.71	4.78	6.45	1.37	0.30
	11	3.89	4.98	6.41		
	31	4.34	5.33	6.86		
62-10	5	5.05	6.32	9.41	2.18	0.91
	73	4.56	5.97	9.00	2.22	0.81
	138	4.58	5.82	9.81	2.62	1.38
62-14	5	4.56	5.41	7.14	1.29	0.44
	15	4.58	5.42	7.05	1.24	0.40
62-15	5	4.58	5.82	9.81	2.62	1.38
	75	4.50	6.68	9.35	2.43	0.25
	121	3.95	5.08	7.10	1.58	0.45
62-19	5	3.73	4.80	6.57	1.42	0.35
	72	3.10	3.98	7.10	2.00	1.12
	118	4.55	5.54	7.86	1.66	0.67
62-20	5	4.94	5.95	9.00	2.03	1.02
	79	5.25	7.40	10.51	2.63	0.48
	130	5.41	8.00	11.98	3.29	0.70
62-21	5	4.26	5.19	6.22	0.98	0.05
	78	4.16	5.41	7.95	1.90	0.65
62-24	3	4.42	5.48	7.85	1.71	0.66
	28	4.89	5.84	10.16	2.63	1.68
	52	5.38	7.76	12.85	3.73	1.35
62-25	2	4.37	5.24	6.55		
	Grab	4.62	5.40	6.66	1.02	0.24
62-28	5	4.51	5.50	7.09	1.29	0.30
	70	4.73	5.80	8.85	2.06	0.99
62-32	2	4.63	5.50	7.25		
62-33	Grab	4.32	5.33	7.04	1.36	0.35

TABLE I

Particle size analyses of near-flank sediments (Cont'd)

Core No.	Depth in Core (cm)	Q1 $\phi$	Md $\phi$	Q3 $\phi$	QD $\phi$	Skq $\phi$
62-34	3	5.45	7.10	9.32	1.94	0.29
	68	5.45	7.60	10.63	2.59	0.44
	146	7.54	8.70	9.86	1.16	0.00
62-35	Grab	5.32	6.60	9.00	1.84	1.12
62-36	3	5.05	6.25	8.57	1.76	0.56
	34	4.30	5.25	7.85	1.78	0.83
	72	5.27	7.00	9.75	2.24	0.51
62-37	3	5.65	7.25	9.18	1.77	0.17
	35	4.00	6.20	9.10	2.55	0.35
	57	5.05	6.70	9.70	2.32	0.68
62-38	5	4.98	6.52	8.22	1.92	-0.38
	35	5.04	6.70	9.10	2.03	0.37
62-39	4	4.98	6.50	8.90	1.96	0.44
	11	3.96	5.55	10.40	3.22	1.63
	48	4.77	6.76	9.52	2.38	0.39
	90	5.55	7.85	10.38	2.41	0.12
62-57	10	6.83	8.52	10.25	1.71	0.02
	74	4.26	6.00	11.20	3.47	1.73
	145	4.93	5.79	8.85	1.96	1.10
62-58	3	5.10	6.56	9.20	2.05	0.59
	91	4.74	6.06	8.85	2.07	0.75
61-1	3	5.12	5.98	9.00	1.94	1.08
	47	4.83	5.95	9.50	2.34	1.22
	57	4.99	6.80	10.37	2.69	0.88
61-9	5	4.56	6.17	8.43	1.94	0.32
	15	4.62	5.75	9.15	2.27	1.14
	48	4.71	5.38	7.56	1.43	0.76
	57	5.12	6.15	10.20	2.54	1.51
61-10	5	5.05	6.00	8.44	1.70	0.74
	25	5.24	6.29	9.00	1.88	0.83
61-18	5	5.51	6.68	8.91	1.70	0.53
	45	5.44	6.76	9.26	1.91	0.59
	55	5.42	7.02	10.78	2.68	1.08
	82	6.78	8.52	11.78	2.50	0.76

Constituents: All material greater than 250 microns in diameter was separated from each subsample used for size analysis and examined under a binocular microscope. This procedure was followed to determine the nature and the source of the sedimentary material and to estimate grossly the abundance of various components present.

Near-flank sand-sized particles are composed predominantly of skeletal and non-skeletal calcium carbonate. The skeletal debris is represented by the tests of planktonic and benthonic foraminifera, pteropods, ostracods, calcareous algae, molluscs, coral debris, alcyonarian spicules, and echnoid spines and plates. Nonskeletal particles are oolites, casts of foraminifera, and oolith-like particles described by Illing (1954) as grains of aragonite matrix. In addition to the calcareous material, small amounts of siliceous sponge spicules were encountered.

In the majority of the near-flank cores fibrous plant-like material is present and serves to aggregate numerous fine particles which ordinarily would fall into a smaller particle-size category.

No visual or mineralogical examination of the material comprising the silt and lutite fraction was made; however, X-ray analysis by Rusnak and Nesteroff (1962) revealed that the finer fraction becomes more calcitic with decreasing grain size, and the less than 2 micron fraction contains about equal amounts of calcite and aragonite.

Placement of this sediment into one of the existing deep-sea sediment classifications after Revelle (1944) or Olausson (1961) is unwarranted as these categorizing schemes were originated for the constituents normally found in deep-sea areas away from rich sources of shallow-water material. Likewise, classification of the sediment under one of the many schemes for shallow-water sediments is not feasible due to the large quantity of deep-sea components. Consequently, the bottom material from the near-flank area will be referred to as calcareous ooze, and no generic implications are attached.

Organic Carbon: Organic carbon content of the top centimeter of the near-flank sediments is high relative to samples from the central area of the TOTO. The lowest value of organic carbon content from near-flank samples was 0.21 percent, the highest 2.48 percent, and the average 1.22 percent. These values are lower than those obtained on the shallow banks surrounding the channels where values range from 3 to 6 percent organic content (Trask, 1955) but are higher than the average deep-sea sediments which contain 0.3 to 1.5 percent total organic matter (Schott, in Trask, 1955).

A strong odor of  $H_2S$  was noticeable from all the near-flank cores. Over half of the cores from this group were measured for hydrogen ion concentration (pH) at the top and bottom immediately after being brought aboard ship, and in all instances the pH was between 6.0 and 7.2. In contrast, cores from the central or axial area show lithologic features indicative of oxidizing rather than reducing conditions.

Mass Physical Properties: Measurements of sediment density, water content, void ratio, and porosity were made, and the results are presented in Table II. In some instances, cores suitable for particle size analysis were not considered suitable for mass

physical properties analyses; consequently, the data for a particular core may appear under one heading and not the other.

TABLE II

Near-flank sediment density, water content, void ratio, and porosity

Core No.	Depth in Core (cm)	Wet Unit Weight (gm/cc)	Water Content (%)	Void Ratio	Porosity (%)
62-1	8	1.53	89.10	1.60	61.53
	27		99.81		
	47	1.54	82.62	2.30	69.69
	71		71.37		
	94	1.60	68.86	1.94	65.98
62-10	14	1.55	82.22	2.27	69.41
	42		61.34		
	73	1.63	68.08	1.87	65.16
	108		74.06		
	138	1.65	74.06	1.76	63.76
62-15	15	1.73	52.79	1.46	59.34
	43		55.40		
	75	1.80	50.98	1.32	57.08
	98		59.29		
	121	1.77	46.51	1.30	56.52
62-19	11	1.58	69.90	1.99	66.55
	30		75.94		
	72	1.59	71.62	1.99	66.55
	88		90.44		
	118	1.63	62.28	1.77	63.89
62-20	31	1.66	58.94	1.66	62.40
	56		61.62		
	79	1.63	64.14	1.80	64.28
	105		72.73		
	130	1.60	71.73	1.99	66.55
62-21	18	1.60	67.82	1.92	65.75
	48		66.75		
	78	1.64	63.33	1.77	63.89
	100		61.45		
	136	1.66	68.71	1.83	64.66
62-24	3	1.63	66.77	1.84	64.78
	16		65.12		
	28	1.61	63.49	1.83	64.66
	39		59.78		
	52	1.63	61.41	1.76	63.76

TABLE II

Near-flank sediment density, water content, void ratio, and porosity (Cont'd)

Core No.	Depth in Core (cm)	Wet Unit Weight (gm/cc)	Water Content (%)	Void Ratio	Porosity (%)
62-28	13	1.64	63.30	1.77	63.89
	44		60.98		
	70	1.65	61.08	1.72	63.23
	114		60.23		
	142	1.63	66.01	1.84	64.78
62-37	3	1.72	129.89	2.72	73.11
	27		74.62		
	33		38.80		
	34		88.69		
	59	1.72	46.69	1.37	57.80
62-38	2		74.05		
	26		83.34		
	47		93.24		
62-39	11	1.55	65.85	1.98	66.44
	28		65.90		
	48	1.63	66.04	1.83	64.66
	70		94.75		
	90	1.51	83.01	2.37	70.32
62-57	10	1.50	91.16	2.55	71.83
	43		73.74		
	74	1.69	60.82	1.65	62.26
	113		81.50		
62-58	145	1.69	58.41	1.60	61.53
	3	1.39	121.92	3.44	77.47
	26		113.89		
	46	1.47	97.79	2.75	73.33
	69		85.72		
	91	1.53	79.45	2.26	69.32
61-1	3	1.72	56.09	1.53	60.47
	16		56.84		
	28	1.72	56.00	1.55	60.78
	37	1.79	48.85	1.32	56.89
	47		47.48		
61-9	5	1.59	72.18	2.01	66.77
	15	1.67	59.77	1.66	62.40
	46	1.70	54.64	1.53	60.47
	57	1.70	60.30	1.62	61.83
61-18	5	1.34	92.15	2.98	74.87
	17	1.55	83.68	2.29	69.60
	23		72.57		
	35		80.94		
	45	1.54	79.26	2.24	69.13
	55		81.10		

Density measurements were obtained by inserting a chrome cylinder of known weight and volume into the core and extruding the core from the liner for a distance equal to the length of the cylinder. After trimming and wiping the exterior and ends of the cylinder clean of excess sediment, the weight of the sediment and its container were obtained. This procedure measured the wet unit weight of the sedimentary material.

Water content of the sediment was measured by longitudinally splitting the increment used in the density measurement, extracting a sufficient quantity of the sediment from the center of the increment, weighing the sample immediately, drying at 105°C, and reweighing. The water content was calculated by the equation:

$$\text{Water Content, } w(\%), = \frac{(\text{Wet Weight} - \text{Dry Weight})}{\text{Dry Weight}} \times 100.$$

The void ratio was determined by the equation:

$$\text{Void Ratio, } e, = \frac{V_v}{V_s}$$

where  $V_s = \frac{\text{Dry Bulk Density}}{\text{Specific Gravity}}$

and  $V_v = 1 - V_s.$

Porosity of the sediment was obtained by the equation:

$$\text{Porosity } (\%) = \frac{V_v}{\text{Total Volume}} \times 100 = \frac{e}{1+e}.$$

The values presented in Table II show approximately 70 percent of the cores in the near-flank area decreasing in water content, void ratio, and porosity with depth in the sediment and increasing in density with depth. However, particle grain size is strikingly similar through the sediment, and the mineralogical composition is almost wholly  $\text{CaCO}_3$ . The increase in density with depth in the sediment is most likely the result of compaction and consequent loss of interstitial water.

Below are the maximum, minimum, and average values of the properties tabulated in Table II:

Property	Maximum	Minimum	Average
Wet Unit Weight	1.80	1.34	1.62
Water Content	129.8	47.4	70.4
Void Ratio	2.98	1.30	1.93
Porosity	77.5	56.5	65.2



## Axial Sediments

Bottom samples representing axial sediments are from the relatively flat area located at the base of the flanks of the channel in the narrow, elongated portion of the TOTO north of the cul-de-sac (Fig 6). Compared to near-flank sediments, axial sediments are characterized by lighter, more varied color, a wider range of particle grain size, higher density, lower water and organic carbon content, and many abrupt changes in lithology with depth in the sediment. Cores 62-60 through 62-63, which are from Northeast Providence Channel, are included herein because of their similarity to axial sediments.

Cores included within the axial category are:

62-2	62-22	62-50	61-6
62-3	62-23	62-51	61-7
62-5	62-27	62-52	61-8
62-7	62-29	62-60	61-21
62-8	62-30	62-61	61-22
62-13	62-31	62-62	
62-16	62-47	62-63	
62-17	62-48	61-2	
62-18	62-49	61-4	

Samples from the central reaches of the channel show frequent, abrupt changes in sediment color with depth in the core (Fig 8). Colors range from dark yellowish brown (10YR6/6) to a pure white (N9), and, in the majority of instances, the color changes do not appear related to a change in any particular sedimentary property. Colors in the orange hue are prevalent and are believed to represent oxidation of the ferrous ions present in the sediment. As opposed to the near-flank sediments, no  $H_2S$  odor was detected in the axial sediments, and the few pH measurements taken were always in excess of 7.0. Superimposed on the colors recorded in Figure 8 are occasional bluish-black mottles and streaks throughout the majority of the cores which are probably due to decomposition of plant debris incorporated in the sediment. Plate I compares a typical core from the axial and near-flank area.

Almost all axial cores contain relatively coarse-grained layers oriented normal to the core axis. These layers are in sharp contrast with the underlying material, grade gradually into the overlying material, and show a gradation from coarse to fine sediments upward in the core. Plate II is an example of this type deposit, and core 61-21 in Figure 8 shows the decrease in median grain size diameter upwards in one of the graded beds. In a few of the cores the coarse layers are only slightly coarser than the surrounding material, and, as a result, in a freshly split core the upper portion of the graded sequences are difficult to recognize. However, on drying, the decrease in particle size upwards becomes conspicuous, and, as discussed by Ericson et al (1961), the shrinkage of such sediment on drying is proportional to the ratio of  $\frac{1}{d^2}$  particles to larger grains. In effect, the differential shrinkage of the sediment when thoroughly dry produces a smoothly tapered increment where the base of the sequence (due to less contraction) is wider than the upper portion of the layer where it makes contact with the overlying sediment.

Cause of graded bedding similar to that present in the TOTO sediments is discussed by Kuenen (1953) and Kuenen and Menard (1952), and lithologic features of this nature are suspected to be the result of deposition by turbidity currents of high density. Such processes are of short temporal duration, and the velocity attained by the turbid flow is dependent upon the density of the flow and the slope gradient over which it is passing. As the turbidity current decreases in velocity, the coarser and gradually the finer and finer particles are deposited; hence, vertical grading results. Graded beds of this nature and the suspected mode of deposition have been designated by Kuenen (1957) as "turbidites," and this nomenclature will be used herein.

Turbidites do not generally occur at the same depth level in all cores, or are they of the same vertical thickness. Since all cores except those preceded by the number 61 were taken with the same instrument and following the same method, differentially induced compaction through variation in sampling procedure or instrument type is not suspected for the lack of correlation between turbidites from one core to another. To account for the lack of horizontal continuity, extensive sheet-like turbidity currents are not theorized. Instead, localized turbidity flows within the many gullies trending at right angles to the bank edges and incising the channel walls are more likely. High velocity restricted flows of this nature are discussed by Ericson et al (1961), and such localized transporting phenomena which have originated through slumping on the upper walls or bank edges best explain the discontinuous, variable distribution of the turbidites. Rusnak and Nesteroff (1962) discussed the TOTO turbidites in detail and concluded that 70 to 90 percent of the channel deposits have been produced by turbidity currents.

It is stated in a Technical Report by the University of Miami (1958) that density (turbidity) currents created by instability of sediments on the edge of the banks may contribute material to the floor of the TOTO. Many of the cores in the near-flank area were collected from within the gullies and displayed no features suggestive of turbidity current deposition. Consequently, it is expected that the turbidity currents originating on the banks above the near-flank area flow with sufficient velocity down-slope to prohibit deposition in this area. On the other hand, turbidity flows may be originating near the base of the flanks and flowing outward into the channel, thereby accounting for the absence of turbidities in the near-flank sediments.

Particle Size: Silt-sized particles are the dominant size fraction in the axial sediments; however, compared to the near-flank area, there is a decrease in percentage of silts, a slight increase in sands (generally explained by the coarse turbidite layers present), and a fairly large increase in lutites (Table III). Average particle size distribution in the axial area is 17 percent sand, 49 percent silt, and 34 percent lutite.

Sorting values are higher in these sediments as a result of an increase in sand and lutite. Over 75 percent of the samples analyzed are poorly sorted, and the bulk of the remaining samples show average sorting. Sorting values in the turbidites are generally high. Rusnak and Nesteroff (1962) discussed sorting coefficients and explained the poor sorting in the turbidites as relating to the small size of the channel which limits the distance over which sorting can occur and to the hydraulic behavior of the variety of biological debris in the turbidity current flow.

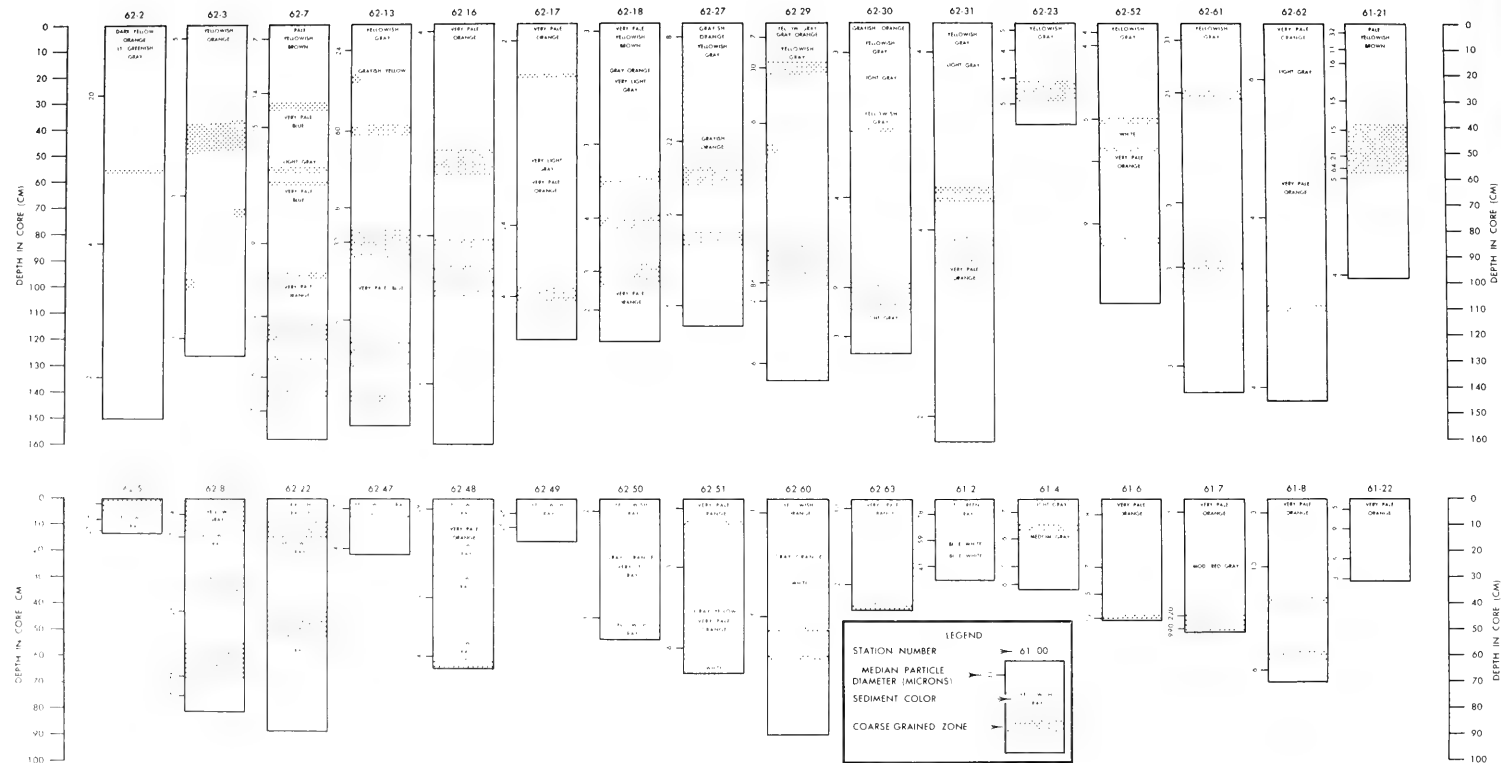


FIGURE 6. LONGITUDINAL CROSS SECTION OF AXIAL CORES



TABLE III  
Particle size analyses of axial sediments

Core No.	Depth in Core (cm)	Q1 $\phi$	Md $\phi$	Q3 $\phi$	QD $\phi$	Skq $\phi$
62-2	27	3.94	5.68	8.09	2.08	0.34
	84	5.23	7.92	11.99	3.38	0.69
	136	5.74	8.90	12.33	3.30	-0.87
62-3	5	6.58	8.24	10.45	1.94	0.28
	43	5.01	7.64	11.67	3.33	0.70
	65	5.43	8.30	11.67	3.12	0.25
	120	7.53	8.45	11.46	2.87	0.15
62-5	2	1.75	2.67	4.45	1.35	0.43
	8	3.43	4.93	6.90	1.24	0.24
	12	3.32	5.17	7.48	2.08	0.73
62-7	5	5.33	7.08	10.00	2.34	0.37
	32	5.12	5.92	9.19	2.04	1.24
	44	4.28	5.93	9.59	2.66	1.01
	88	5.04	6.84	10.00	2.48	0.68
	117	5.58	9.00	11.80	3.11	-0.31
	140	2.99	5.95	9.44	3.23	0.27
	154	4.83	7.20	9.94	2.56	0.19
62-8	5	3.77	4.89	6.75	1.49	0.37
	14	3.96	5.24	7.62	1.83	0.55
	42	4.05	5.30	8.05	2.00	0.75
	67	3.21	3.72	5.13	0.96	0.40
	74	4.86	6.14	10.02	2.58	1.30
62-13	9	4.62	5.40	7.17	1.28	0.50
	40	3.50	4.12	5.91	1.20	0.59
	70	4.94	7.00	10.49	2.78	0.72
	83	3.44	5.05	8.25	2.41	0.80
	134	5.02	6.95	10.57	2.78	0.85
62-16	2	5.40	7.67	10.90	2.75	0.48
	7	5.75	8.13	10.91	2.58	0.20
	80	5.98	8.56	11.20	2.62	0.04
	156	6.41	9.21	11.99	2.79	-0.01
62-17	5	5.70	8.13	11.01	2.66	0.24
	76	5.29	9.20	15.85	5.28	1.37
	103	3.46	5.40	9.42	2.98	1.04

TABLE III

Particle size analyses of axial sediments (Cont'd)

Core No.	Depth in Core (cm)	Q1 $\phi$	Md $\phi$	Q3 $\phi$	QD $\phi$	Skq $\phi$
62-18	3	6.00	8.54	10.94	2.47	-0.07
	46	5.66	8.50	11.77	3.06	4.22
	76	5.05	7.90	11.19	3.07	0.22
	94	5.45	8.15	10.95	3.59	0.32
	109	5.08	8.85	12.75	2.75	0.05
62-23	1	5.64	7.62	9.78	2.07	0.09
	3	5.56	7.61	9.00	1.72	-0.33
	11	5.58	8.00	10.86	2.64	-0.28
	21	5.32	7.93	10.99	2.84	0.22
	36	5.31	7.82	10.05	2.37	-0.14
62-27	5	5.11	6.85	9.95	2.42	0.63
	45	3.48	5.51	9.82	3.17	0.94
	73	5.24	7.57	10.75	2.76	0.43
	108	4.79	7.80	11.16	3.19	0.18
62-29	5	5.23	7.23	11.45	3.11	1.11
	17	4.22	5.11	6.00	0.89	0.00
	38	4.79	6.00	10.10	2.66	1.44
	99	2.66	3.56	5.43	1.39	0.49
	106	5.79	9.25	11.58	2.90	-0.57
	129	5.19	7.50	10.56	2.69	0.38
62-30	11	6.00	8.08	10.15	2.07	-0.01
	66	2.54	6.76	10.12	3.79	-0.43
	101	5.72	9.00	11.30	2.76	-0.98
	120	5.35	8.49	11.35	2.80	0.07
62-31	10	5.80	8.13	10.73	2.47	0.14
	78	4.98	7.98	11.81	3.42	0.42
	149	5.33	8.81	13.55	4.11	0.63
62-47	3	4.43	5.85	9.50	2.54	1.12
	19	5.57	7.96	10.86	2.65	0.26
62-48	3	4.09	5.35	8.15	2.03	0.77
	51	4.00	5.70	9.60	2.80	0.90
	91	1.46	2.42	3.26	2.18	0.83
	101	5.00	8.02	9.90	2.45	-0.57
62-49	5	4.42	5.30	6.58	1.08	0.20
	10	4.51	5.35	7.16	1.33	0.49

TABLE III

Particle size analyses of axial sediments (Cont'd)

Core No.	Depth in Core (cm)	Q1 $\phi$	Md $\phi$	Q3 $\phi$	QD $\phi$	Skq $\phi$
62-50C	4	6.00	8.80	11.67	2.84	0.04
	44	7.35	11.20	15.15	3.90	0.05
62-51	3	5.53	7.74	10.59	2.53	0.32
	25	5.56	8.31	11.60	3.02	0.27
	56	5.21	7.48	9.86	2.33	0.06
62-52A	3	5.68	7.86	10.00	2.16	0.48
	8	5.43	7.52	10.55	2.56	0.47
	52	5.58	8.25	10.83	2.63	-0.05
	76	4.99	6.75	9.58	2.30	0.54
62-60	5	4.91	6.54	9.44	2.27	0.64
	42	5.00	6.08	7.14	1.07	-0.01
62-61	6	3.55	5.05	7.95	2.20	0.70
	26	4.06	5.60	9.18	2.56	1.02
	68	3.78	5.26	8.79	2.51	1.03
	93	3.43	5.25	8.78	2.68	0.86
	133	5.35	8.35	13.87	4.26	1.26
62-62	20	5.36	7.30	11.08	2.86	0.92
	73	5.14	8.25	12.45	3.66	0.55
	138	5.42	7.90	11.64	3.11	0.63
62-63	3	5.01	6.70	10.05	2.52	0.83
	32	5.50	9.23	14.10	4.30	0.57
61-2	5	3.17	3.73	5.88	1.36	0.80
	15	2.66	4.07	6.65	2.00	0.59
	25	2.90	4.56	7.54	2.32	0.66
61-4	5	5.42	7.13	9.99	2.29	0.58
	15	5.65	7.49	9.66	2.01	0.17
	25	6.07	7.80	10.67	2.30	0.57
	32	5.47	7.28	10.75	2.64	0.83
61-6	5	5.72	7.02	10.02	2.15	0.85
	25	5.57	7.15	10.58	2.51	0.93
	35	5.80	7.62	11.40	2.80	0.98
	45	4.84	6.33	10.50	2.83	1.34
61-7	5	6.06	7.59	9.78	1.86	0.33
	45	0.15	2.19	4.32	2.09	0.05
	50	-2.13	-1.71	5.41	-1.12	-0.10

TABLE III

Particle size analyses of axial sediments (Cont'd)

Core No.	Depth in Core (cm)	Q1 $\phi$	Md $\phi$	Q3 $\phi$	QD $\phi$	Skq $\phi$
61-8	5	6.89	8.52	11.11	2.11	0.48
	25	5.02	6.55	11.55	3.27	1.74
	65	5.22	7.30	10.73	2.76	0.68
61-21	3	3.93	4.74	8.15	2.11	1.30
	10	4.30	6.46	8.60	2.15	0.01
	15	3.55	6.01	8.53	2.49	0.03
	29	3.54	6.09	8.64	2.55	0.00
	40	4.90	7.31	9.72	2.41	0.00
	50	2.50	5.69	8.88	3.19	0.00
	55	0.28	3.87	7.45	3.59	0.00
	59	5.27	7.63	9.99	2.36	0.00
	96	5.51	7.99	13.12	3.81	1.33
61-22B	4	4.99	6.20	9.00	2.01	0.80
	12	5.26	6.85	10.59	2.67	1.08
	22	5.95	7.77	11.74	2.90	1.08
	30	6.39	8.43	12.30	2.96	0.92

Skewness values are predominantly positive; however, proportionally more samples are skewed in a negative direction, and the skewness values more closely approach zero than near-flank sediments.

**Constituents:** Ungraded sections of the axial cores are dominated by planktonic foraminifera and pteropods; although, reef-derived material is present to some degree. The turbidites are composed in equal part of pelagic and reef-derived materials. Pteropods present in the graded beds are dominated by the genera Creseis (the tapered needlelike form observable in Plate II).

Core 62-8 contained a number of both clear and smoky angular quartz particles which were not encountered in any other core. Source area of the quartz is unknown but could be explained through transport by winds from a terrestrial continental source; although, wider distribution of the anomalous particles would then be expected.

**Organic Carbon:** Organic carbon content in the axial cores averages 0.44 percent and is about 1 percent lower than the average for near-flank sediments. The majority of cores show a sharp decrease in organic content with depth. The maximum value encountered was only 1.08 percent.

Vasicek (in Ericson et al, 1961) advanced the theory that turbidity currents rushing down slope should sweep up or carry along much living or dead matter which would be deposited with the finer fraction. Previously Ericson et al (1952) reported the common



occurrence of plant debris and hydrotroilite (an amorphous monosulfide of iron  $\text{FeS} \cdot \text{H}_2\text{O}$ ) in ungraded beds within cores from the North Atlantic. However, it can be shown that no evidence of organic entrapment is present in the graded portions of axial sediments, and organic carbon values from turbidites in this area follow the general decrease in organic matter with depth found throughout the sediment.

Mass Physical Properties: Axial cores display relationships between physical properties with depth in the sediment which are similar to the near-flank group. Sediment density generally increases with depth; conversely, water content, void ratio, and porosity values generally decrease with depth.

Table IV shows the sediment from this area to be slightly denser and considerably lower in water content, void ratio, and porosity than near-flank sediments. In addition, the axial group shows less magnitude of variation of these values around the mean.

Below are the maximum, minimum, and average values of the properties tabulated in Table IV:

Property	Maximum	Minimum	Average
Wet Unit Weight	1.76	1.53	1.66
Water Content	89.1	44.5	66.9
Void Ratio	2.58	1.35	1.75
Porosity	72.1	56.3	63.0

#### Cul-de-sac Sediments

Bottom samples representing cul-de-sac sediments are from the flat, central area of the cul-de-sac and the flanks bounding the northern and northeastern portion of this area (Fig 6). Cores from the central portion of the cul-de-sac are differentiated from near-flank and axial cores by more frequent turbidites, poorer sorting, lower density, higher water and organic carbon content, a high void ratio, and a higher porosity.

Cores included in this group are:

62-40	62-45	62-56
62-41	62-46	62-59
62-42	62-53	61-11
62-43	62-54	61-12
62-44	62-55	61-16

Cores 62-45, 62-46, 62-44, 62-53, and 62-55 are arbitrarily included in the cul-de-sac group because of variations in color and the presence of a few recognizable turbidites; however, these cores are very similar to near-flank cores and the difference between the two is slight.

TABLE IV

Axial sediment density, water content, void ratio, and porosity

Core No.	Depth in Core (cm)	Wet Unit Weight (gm/cc)	Water Content (%)	Void Ratio	Porosity (%)
62-2	27	1.71	54.90	1.52	60.31
	60		94.33		
	85	1.64	63.94	1.78	64.02
	112		56.12		
	137	1.66	59.69	1.68	62.68
62-3	20	1.69	62.13	1.67	62.54
	46		58.21		
	65	1.66	58.54	1.65	62.26
	93		58.26		
	120	1.67	57.84	1.63	61.97
62-7	44	1.67	59.24	1.65	62.26
	67		72.23		
	88	1.71	58.15	1.57	61.08
	112		59.35		
	147	1.65	63.19	1.76	63.76
62-8	14	1.65	59.24	1.68	62.68
	26		72.23		
	42	1.64	58.15	1.70	62.96
	55		59.35		
	74	1.64	63.19	1.76	63.76
62-13	9	1.64	71.17	1.90	65.51
	45		66.06		
	70	1.71	53.31	1.49	59.83
	101		64.39		
	134	1.72	50.68	1.43	58.84
62-16	3	1.63	68.25	1.87	65.15
	46		60.05		
	80	1.62	65.29	1.83	64.66
	115		69.35		
	156	1.66			
62-17	28	1.64	69.89	1.88	65.27
	52		60.78		
	76	1.66	58.50	1.65	62.26
	93		56.85		
	113	1.67	55.34	1.58	61.24

TABLE IV

Axial sediment density, water content, void ratio, and porosity (Cont'd)

Core No.	Depth in Core (cm)	Wet Unit Weight (gm/cc)	Water Content (%)	Void Ratio	Porosity (%)
62-18	3	1.58	82.94	2.22	68.94
	28		72.75		
	46	1.66	64.31	1.76	63.76
	80		66.25		
	109	1.66	64.20	1.75	63.63
62-22	3	1.57	87.23	2.31	69.78
	22		67.25		
	42	1.58	76.77	2.12	67.94
	61		69.92		
	78	1.67	48.36	1.47	59.51
62-27	16	1.68	55.27	1.57	61.08
	32		69.62		
	56	1.68	53.54	1.54	60.62
	90		53.75		
	108	1.73	54.14	1.48	59.67
62-29	38	1.59	60.61	1.65	62.26
	71		69.03		
	104	1.56	77.24	2.16	68.35
	129	1.67	58.02	1.63	61.97
62-30	11	1.68	116.35	2.58	72.06
	44		26.81		
	66	1.70	60.21	1.62	61.83
	93		70.81		
	120	1.69	61.24	1.65	62.26
62-31	10	1.60	67.50	1.91	65.63
	45		79.02		
	78	1.70	56.22	1.55	60.78
	123		55.28		
	149	1.74	49.04	1.38	57.98
62-47	3	1.65	61.52	1.73	63.36
62-48	3	1.74	61.25	1.51	60.15
	27		50.54		
	51	1.74	51.88	1.29	56.33
	76		60.65		
	101	1.57	54.82	2.11	67.84
62-49	3	1.75	48.15	1.35	57.44

TABLE IV

Axial sediment density, water content, void ratio, and porosity (Cont'd)

Core No.	Depth in Core (cm)	Wet Unit Weight (gm/cc)	Water Content (%)	Void Ratio	Porosity (%)
62-50	3	1.58	89.17	2.33	69.96
	24		62.86		
	44	1.64	64.75	1.79	64.14
62-51B	3	1.64	72.06	1.92	65.75
	25	1.65	65.13	1.79	64.15
	56	1.68	54.74	1.56	60.93
62-52A	3	1.59	87.56	2.28	69.51
	31		68.38		
	52	1.68	59.10	1.63	61.97
	73		52.73		
	97	1.74	49.19	1.39	58.15
62-60	16	1.70	56.71	1.56	60.93
	29		55.02		
	41	1.70	61.20	1.64	62.12
	64		59.29		
	82	1.72	53.57	1.48	59.67
62-61	6	1.67	60.18	1.67	62.54
	38		54.21		
	68	1.72	55.01	1.51	60.15
	100		55.27		
	133	1.70	55.75	1.80	64.28
62-62	9	1.69	62.76	1.68	62.68
	44		56.06		
	73	1.65	56.86	1.65	62.26
	105		55.47		
	138	1.65	59.74	1.69	62.82
62-63	5	1.64	75.41	1.98	66.44
	17		59.12		
	32	1.66	61.75	1.71	63.09
61-2	6	1.70	60.90	1.63	61.97
	15	1.68	61.55	1.67	62.54
	22		58.79		
61-4	5	1.62	70.33	1.92	65.75
	15	1.68	61.87	1.68	62.68
	25	1.65	80.76	2.05	67.21

TABLE IV

Axial sediment density, water content, void ratio, and porosity (Cont'd)

Core No.	Depth in Core (cm)	Wet Unit Weight (gm/cc)	Water Content (%)	Void Ratio	Porosity (%)
61-6	5	1.67	62.05	1.70	62.96
	16		58.25		
	25	1.65	63.58	1.76	67.76
	35	1.65	65.08	1.79	64.15
	44		65.18		
61-7	5	1.65	63.00	1.75	63.66
	25	1.66	63.68	1.74	63.50
	35		44.47		
61-8	5	1.53	85.51	2.37	70.32
	25	1.66	64.94	1.76	67.76
	45	1.64	65.67	1.81	64.41
	56	1.65			
61-21	3	1.69	56.76	1.58	61.24
	12	1.66	64.86	1.76	63.76
	21	1.69	59.30	1.62	61.83
	29	1.69	62.73	1.67	63.54
	48	1.71	54.67	1.51	60.15
	56	1.68	55.14	1.56	60.93
	68	1.71	59.06	1.58	61.24
	76	1.73	56.72	1.52	60.31
61-22B	4		51.99		
	11	1.73	53.83	1.47	59.51
	20		58.36		
	29		60.74		

Longitudinal cross sections of cul-de-sac cores are presented in Figure 9, and, from this figure, the cores collected from the central, flat reaches of this area can be seen to consist almost in equal part of turbidites and sediments laid down particle-by-particle from the water column. Turbidites in this area accounted for well over 40 percent of the sediment column sampled. In the cul-de-sac it was difficult to ascertain the upper contact of turbidites with the overlying sediment; hence, it is possible that a larger percentage of the sediment column is due to turbidity currents than the data reveals.

Many of the cul-de-sac cores gave off a strong  $H_2S$  odor, and the few pH measurements taken were less than 7.0.

Excluding zones of turbidite occurrences, cores from throughout the cul-de-sac are similar in texture and color to near-flank cores, and the portion of these cores attributable to pelagic type sedimentation is strikingly similar to the near-flank area. The top 2 or 3 centimeters of almost all cul-de-sac cores show an orange-red hue which is indicative of oxidizing conditions at the surface and which is absent throughout the remainder of the sediment with depth. Core 62-46 contains a very coarse zone unlike a typical turbidite in that the zone shows no grading but consists of a reef detritus where both the top and bottom contact with the enclosing sediment is sharp. This particular sequence is probably the result of sand "falls" over the bank edges rather than turbidity current deposition.

Particle Size: Silt is the dominant size fraction in this area as well as the remainder of the TOTO; however, the increase in turbidites compared to the axial area raises the percentage of sand by a slight amount. The graded nature of turbidites is apparent in cores 62-42 and 61-16 (Fig 9) where a decrease in median grain diameter upwards in turbidite zones in the core is observable. The average size distribution of the samples analyzed is 20 percent sand, 29 percent silt, and 51 percent lutite.

Poor sorting is prevalent among these sediments, although a few of the samples analyzed from the bottom of the coarser turbidites show almost perfect sorting. Skewness values are not much different than the axial sediments in that the majority of samples are positively skewed with a few negative values present (Table V).

Constituents: Constituents comprising the cul-de-sac sediments are not unlike the other areas of the channel. Turbidites, however, contain a greater percentage of reef-derived material, and oolites and oolith-like particles constitute a major portion of the reef detritus. Plant debris is more prevalent throughout cul-de-sac sediments than in the axial area, and several turbidites contain thin zones of this fibrous material incorporated into the sequence.

Organic Carbon: Organic carbon content of the sediment in this area is the highest encountered in the channel and is probably due to the increase in plant detritus. Surface values of organic carbon are as high as 2.00 percent and decrease in the channel.

Mass Physical Properties: Sediments in the cul-de-sac are less dense and contain a higher water content than any sediments in the TOTO, and, in like manner, void ratio and porosity values are also highest. Although the water content shows a decrease from top to bottom in the cores, there are interruptions in a uniform decrease with depth which are probably due to the large amounts of coarse-grained turbidites present. The turbidites, being more porous, are capable of holding greater water content than the fine-grained material above and below.

As in the other TOTO cores, sediment density generally increases while void ratio and porosity decrease with depth in the sediment.

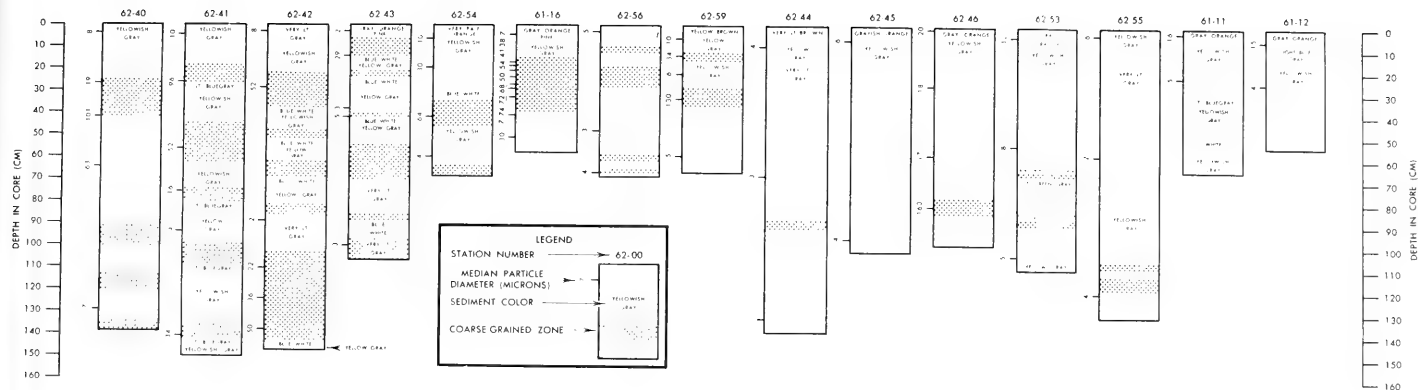


FIGURE 9 LONG TUDINAL CROSS SECTION OF CUL-DE-SAC CORES





TABLE V

Particle size analysis of cul-de-sac sediments

Core No.	Depth in Core (cm)	Q1 $\phi$	Md $\phi$	Q3 $\phi$	QD $\phi$	Sk $\phi$
62-40	5	5.35	6.94	9.36	2.06	0.47
	26	4.70	5.76	8.40	1.90	0.79
	42	1.94	3.19	5.30	1.68	0.43
	65	1.09	4.00	6.87	2.89	-0.02
	129	5.25	7.10	10.38	2.57	0.72
62-41	3	5.37	6.65	8.53	1.58	0.30
	25	2.21	3.37	5.15	1.47	0.31
	56	3.59	4.29	5.62	1.02	0.32
	75	4.95	5.98	9.50	2.28	1.25
	93	6.32	8.27	10.25	1.97	0.02
	141	1.92	4.75	7.57	2.83	-0.01
62-42	3	5.53	7.12	9.43	1.95	0.36
	27	3.58	4.32	5.56	0.99	0.25
	88	5.58	8.85	12.85	3.64	0.37
	111	4.63	5.48	8.89	2.13	1.28
	123	3.92	4.80	5.74	0.91	0.03
	137	3.63	4.32	5.87	1.12	0.43
62-43	3	5.94	8.66	11.45	2.76	0.04
	13	3.93	5.12	7.70	1.89	0.70
	37	5.55	8.50	12.79	3.62	0.67
	41	5.58	7.77	10.10	2.26	0.07
	99	5.58	8.50	11.80	3.11	0.19
62-44	8	5.69	8.25	11.15	2.73	0.17
	67	5.45	8.30	12.60	3.58	0.73
	131	5.51	8.28	12.10	3.29	1.05
62-45	6	5.46	7.30	9.76	2.15	0.31
	94	5.59	7.95	10.79	2.60	0.24
62-46	11	4.55	5.69	8.25	1.85	0.71
	26	4.81	5.80	9.30	2.25	1.26
	57	4.62	5.90	10.62	2.95	1.67
	79	0.75	2.60	2.95	0.20	-0.44
62-53	3	5.20	6.60	10.73	2.77	1.37
	52	5.16	6.90	10.83	2.84	1.10
	102	5.15	7.70	12.10	3.48	0.93
62-54	6	5.36	6.73	9.94	2.29	0.92
	19	3.96	5.11	7.40	1.72	0.57
	41	3.39	3.96	5.52	1.07	0.50
	59	5.34	7.85	14.08	4.37	1.86

TABLE V  
Particle size analyses of cul-de-sac sediments (Cont'd)

Core No.	Depth in Core (cm)	Q1 $\phi$	Md $\phi$	Q3 $\phi$	QD $\phi$	Skq $\phi$
62-55	3	5.48	7.44	10.13	2.33	0.37
	58	5.69	8.70	12.23	3.27	0.26
	120	5.41	8.00	10.85	2.72	0.13
62-56	3	5.55	7.65	10.39	2.42	0.32
	47	5.40	8.50	12.95	3.78	0.68
	66	4.86	7.97	11.96	3.55	0.44
62-59	5	5.16	6.64	9.56	2.20	0.72
	12	2.19	4.93	9.80	3.81	1.07
	22	5.22	7.50	12.55	3.67	1.39
	33	1.88	3.00	4.96	1.54	0.42
	59	4.99	7.50	10.85	2.93	0.42
61-11	1	4.85	5.85	9.15	2.15	1.15
	21	6.44	7.96	10.51	2.04	0.52
61-12	5	5.05	6.11	9.40	2.18	1.12
	25	6.40	8.07	11.14	2.37	0.70
61-16	5	5.74	7.09	9.65	1.96	0.60
	17	3.85	4.86	7.31	1.73	0.72
	19	3.55	4.64	7.24	1.85	0.76
	21	2.83	4.16	7.34	2.26	0.92
	24	2.62	4.33	7.77	2.58	0.86
	27	3.18	3.92	7.10	1.96	1.22
	29	2.37	3.79	7.20	2.42	1.00
	35	3.08	3.77	6.35	1.64	0.94
	41	5.82	7.20	9.79	1.98	0.60
	51	3.82	5.08	7.85	2.02	0.76

The maximum, minimum, and average values of properties presented in Table VI are given below:

Property	Maximum	Minimum	Average
Wet Unit Weight	1.75	1.40	1.58
Moisture Content	132.5	38.5	76.7
Void Ratio	3.61	1.20	2.11
Porosity	78.3	54.5	67.0

TABLE VI

Cul-de-sac sediment density, water content, void ratio, and porosity

Core No.	Depth in Core (cm)	Wet Unit Weight (gm/cc)	Water Content (%)	Void Ratio	Porosity (%)
62-40	26	1.55	75.06	2.15	68.25
	46		67.97		
	64	1.62	82.15	2.13	68.05
	106		83.27		
	129	1.51	88.81	2.47	71.18
62-41	3	1.40	132.54	3.61	78.30
	43		103.53		
	75	1.58	84.50	2.25	69.23
	117		90.43		
	141	1.54	70.37	2.08	67.52
62-42	3	1.45	116.87	3.17	76.01
	42		116.89		
	79	1.45	87.27	2.60	72.22
	113		54.73		
	137	1.75	38.46	1.20	54.54
62-43	13	1.64	59.71	1.71	63.09
	34		84.22		
	50	1.63	68.78	1.88	65.27
	71		78.09		
	99	1.65	59.59	1.69	62.82
62-44	8	1.57	76.43	2.13	68.05
	36		73.35		
	67	1.57	77.55	2.15	68.25
	104		75.34		
	131	1.66	61.97	2.31	69.78
62-45	31	1.62	62.32	1.79	64.15
	47		69.77		
	63	1.59	69.85	1.97	66.32
	77		80.43		
	94	1.60	73.67	2.02	66.88
62-46	8		57.24		
	26	1.69	57.17	1.58	61.24
	43		66.24		
	57	1.65	63.82	1.76	63.76

TABLE VI

Cul-de-sac sediment density, water content, void ratio, and porosity (Cont'd)

Core No.	Depth in Core (cm)	Wet Unit Weight (gm/cc)	Water Content (%)	Void Ratio	Porosity (%)
62-53	3	1.54	92.98	2.46	71.09
	26		82.85		
	52	1.66	67.92	1.88	65.27
	78		67.81		
	102	1.51	53.70	1.48	59.67
62-54	19	1.54	66.24	2.00	66.67
	34		68.38		
	59	1.66	63.96	1.75	63.63
62-55	3	1.51	107.86	2.83	73.89
	35		73.57		
	58	1.54	90.18	2.16	68.35
	81		57.74		
	83		60.33		
	120	1.74	49.87	1.39	58.15
62-56	3	1.54	87.69	2.39	70.50
	29		84.26		
	47	1.57	76.35	2.13	68.05
	66	1.71	55.89	1.53	59.28
62-59	22	1.65	64.81	1.78	64.02
	45		66.24		
	59	1.72	52.19	1.46	59.34
61-11	5	1.48	96.44	2.69	72.89
	16	1.42			
	25		105.12		
	35	1.49	100.07	2.73	73.19
	45		86.89		
	53		83.51		
	61		98.80		
61-12	5	1.56	77.05	2.16	68.35
	16		76.43		
	25	1.53	90.57	2.46	71.09
	45		70.73		
61-16	5	1.53			
	51	1.64			

## RATE OF SEDIMENT ACCUMULATION

The following discussion is based on radiocarbon dating of the TOTO sediments by Ostlund et al (1962) and data presented by Rusnak and Nesteroff (1962).

Figure 10 shows the location of a few of the cores dated and the bulk rate of sediment accumulation at these locations. Figure 11 gives the frequency of turbidity current flows at selected locations.

According to Ostlund et al (1962) the rates of sediment accumulation in the TOTO are generally highest on the bank slopes. Those deeper-water cores that show a relatively high rate of accumulation are from the narrower sections of the channel, and, therefore, tend to show a thicker accumulation for a given volume of supplied sediment than is found in the broader reaches of the basin.

The oldest sediment dated by Ostlund et al (1962) in the TOTO was 26,275 years  $\pm$  570 years and was between 132 to 137 centimeters depth in the core. According to a time scale presented by Ericson et al (1961) this date lies within the last glaciation. Ericson et al (1952) reported that Cretaceous sediments overlain by Pleistocene and Recent sediments were encountered in a core taken at 3,383 meters just north of New Providence Island. The authors accounted for the absent series by turbidity current erosion of exposed Cretaceous sediments at a point not far from the core location.

Sediments in the central area of the TOTO, apparently laid down through particle-by-particle deposition, were termed by Rusnak and Nesteroff as pelagic sediments, and they calculated a very slow rate of accumulation for this type sediment. The slow rate of pelagic sediment accumulation becomes apparent by comparing the bulk sediment accumulation per 1,000 years at various locations in Figure 10 against a range of 1.5 to 3.0 centimeters per 1,000 years accumulation attributed to pelagic type sediments. The balance of the sediments not accounted for by particle-by-particle deposition during a 1,000 year period is assigned to turbidity currents. Frequently the turbidites are considerably older than the sediments over which they lie, indicating that an accumulation of reef-derived and pelagic material builds up on the upper slopes of the near-flank area, and, through various causes, is released to flow down slope on top of the material deposited contemporaneously with the buildup of near-flank accumulations.

From Figure 10 the rate of sediment accumulation can be seen to diminish northward along the channel axis; likewise, frequency of turbidity current occurrence also diminishes in the same direction (Fig 11). Consequently, as the present channel floor continuously slopes in a direction coinciding with decreasing sediment accumulation, it is expected that the slope of the channel floor is in large part a depositional gradient, rather than due primarily to some underlying structural mechanism.

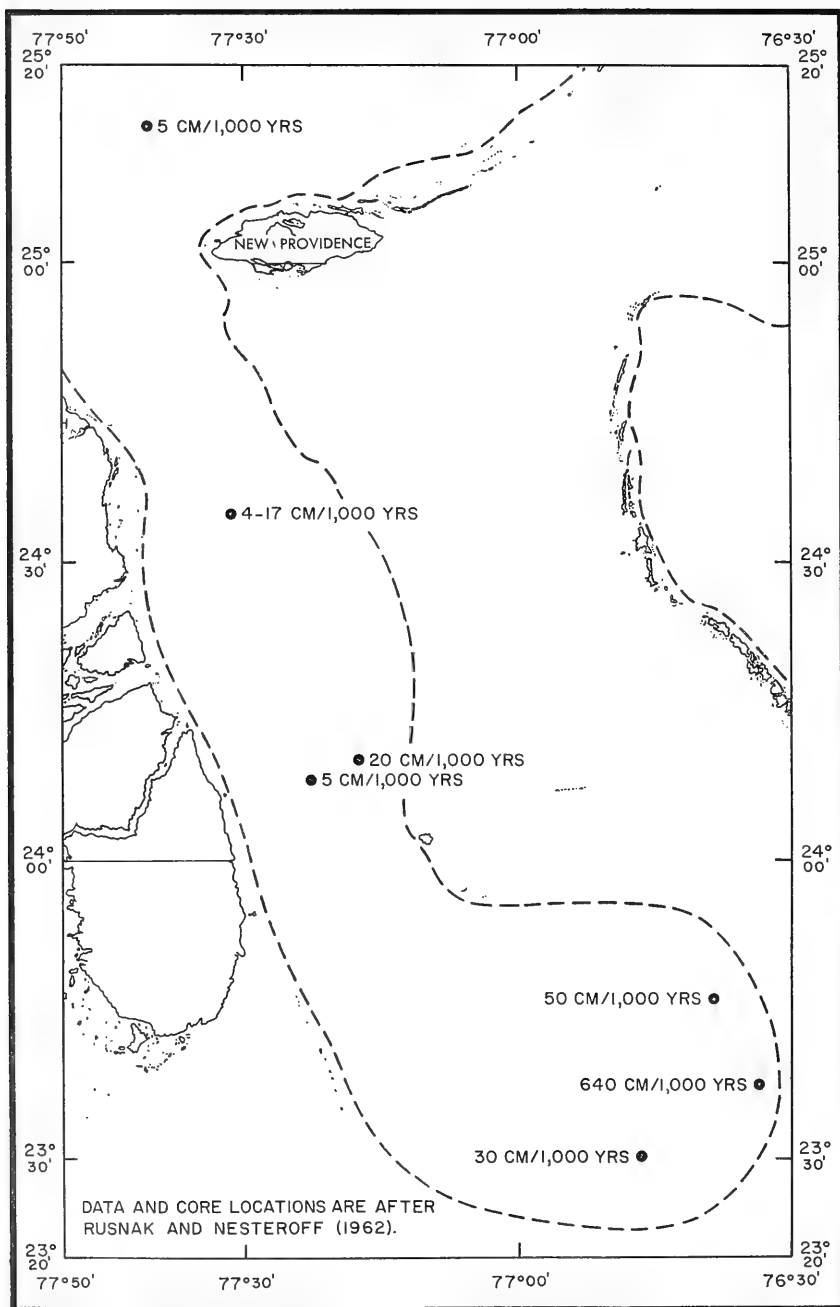


FIGURE 10 RATE OF BULK SEDIMENT ACCUMULATION AT SELECTED LOCATIONS IN THE TOTO

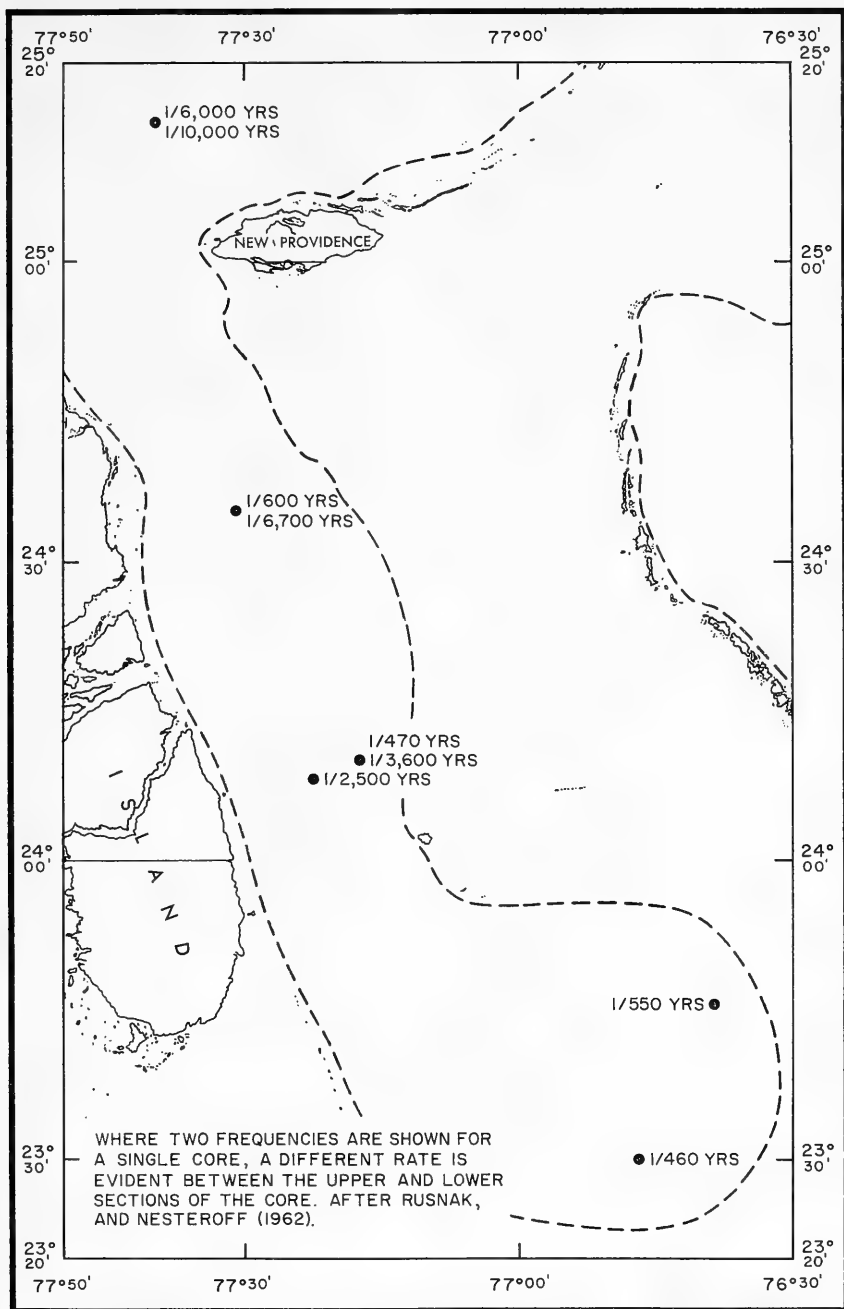


FIGURE 11 FREQUENCY OF TURBIDITY CURRENT FLOWS AT VARIOUS LOCATIONS IN THE TOTO

## ENGINEERING PROPERTIES

### Shear Strength

A test for shearing strength (cohesion) was performed at the top, middle, and bottom of all cores considered to be undisturbed and to have an unaltered water content. Where obvious disturbance of the core had taken place during collection, no shear strength tests were performed; however, in some instances, water content measurements were feasible although the exterior of the core was disturbed.

Shear strength measurements were performed on the same core increments used in the sediment density determinations by carefully extruding the sample from within the cylinder and into the testing device.

The testing procedure is described in detail by Richards (1961) and is only briefly discussed herein. An unconfined compression testing device with plastic platens at either end of an axial rod was used to measure the compressive strength (2 times the shear strength) on sediments of moderate firmness. A stress-strain relationship is obtained by placing an ever increasing load on the upper end of the axial rod with the sediment increment standing upright beneath. Failure of the sample was taken by subsequently plotting the stress-strain data and taking failure at the point of greatest curvature in the plotted line, or arbitrarily, at 20 percent axial strain if the point of greatest curvature was undeterminable.

When the sediment was soupy or not very cohesive, a vane-shear apparatus was used in which a vane was inserted into the sediment and rotated by a constant-speed motor. Degree of vane rotation and degree of applied torque was recorded at the beginning and during the test. Sample failure was determined at the major inflection point of the stress-rotation curve.

The results of the shear strength tests are presented in Table VII and are thought to be sufficiently accurate for most engineering work. Richards (Ibid.) discussed the sources of disturbance to the sediment during the sampling, transporting, and laboratory analysis. Because no information was available to estimate quantitatively the reduction of in-place strength, he concluded that values of shear strength obtained through the method outlined in his report are conservative by an unknown amount compared to in-place strength.

Shear strength or cohesion values were determined in order to calculate the ultimate bearing capacity of the sediment. The ultimate bearing capacity ( $q_u$ ) is defined as the average load per unit area required to produce failure by rupture of a supporting sediment mass, excluding any factor of safety, and is based on the formula:

$$q_u = 1.3 c N_c + w d N_q + 0.4 B w N_\gamma$$



where

$c$  = cohesion,  
 $w$  = buoyant unit weight of the sediment,  
 $d$  = depth to center of sample increment tested,  
 $B$  = width of structure footing, and  
 $N_c$ ,  $N_q$ , and  $N_\gamma$  are bearing capacity factors.

The formula is applicable to structures where the length to width ratio of the base is less than two (square or circular loads) and is usually reduced to  $q_u = 1.3 c N_c$ . Bearing capacity factors are a function of the angle of internal friction. Where the angle is zero (as is assumed for cohesive soils)  $N_c = 5.7$ ,  $N_q = 1.0$ , and  $N_\gamma = 0$  as determined by Terzaghi and Peck (1948).

Results from tests of core number 62-22 will illustrate the application of this formula. If a mass of 35 tons (buoyant weight) with dimensions 12' x 12' x 6' is placed on the bottom at the location of core 62-22 and without impact velocity, the resultant pressure or stress on the sediment would be 486 lbs/ft<sup>2</sup>, and an ultimate bearing capacity of at least the same amount is required for support of the mass. Assuming a surface load of  $q_u = 7.4 c$ , the cohesion necessary for support is 0.46 psi. In core 62-22 the core interval 0 to 7 centimeters has a tested cohesion of 0.53 psi, which (neglecting time) is sufficient for support of the mass.

The majority of cores tested show a large increase in cohesion with depth in the sediment, and inversions, when present, are small in magnitude. Figure 12, which delineates areas in the TOTO of high and low cohesion values, is based on the average cohesion throughout the individual core. From this figure the cul-de-sac sediments, except in two instances, have an average cohesion of less than 1.0 psi, which is the lowest in the channel. Near-flank sediments show a slightly higher cohesion, and axial sediments, except for a zone of less cohesive sediments southeast of Middle Bight, greatly exceed both areas. Although the differences in cohesion values throughout the channel are slight, it might be pointed out that an increase of one unit in the measured cohesion value presented in the example used in core 62-22 above would increase the ultimate bearing strength from 565 to 2,062 lbs/ft<sup>2</sup>.

It is noteworthy that cohesion values follow a trend corresponding to the 3 sedimentary environments delineated in the TOTO. The near-flank and cul-de-sac areas (low cohesion) represent environments of high water content, high organics, low density, and high rates of sediment accumulation, whereas, the axial area (high cohesion) is characterized by relatively low water content, low organics, high density, and low rates of sediment accumulation. Figure 13 delineates values of surface organic carbon content and demonstrates the relationship between organic content and cohesion when compared with Figure 12.

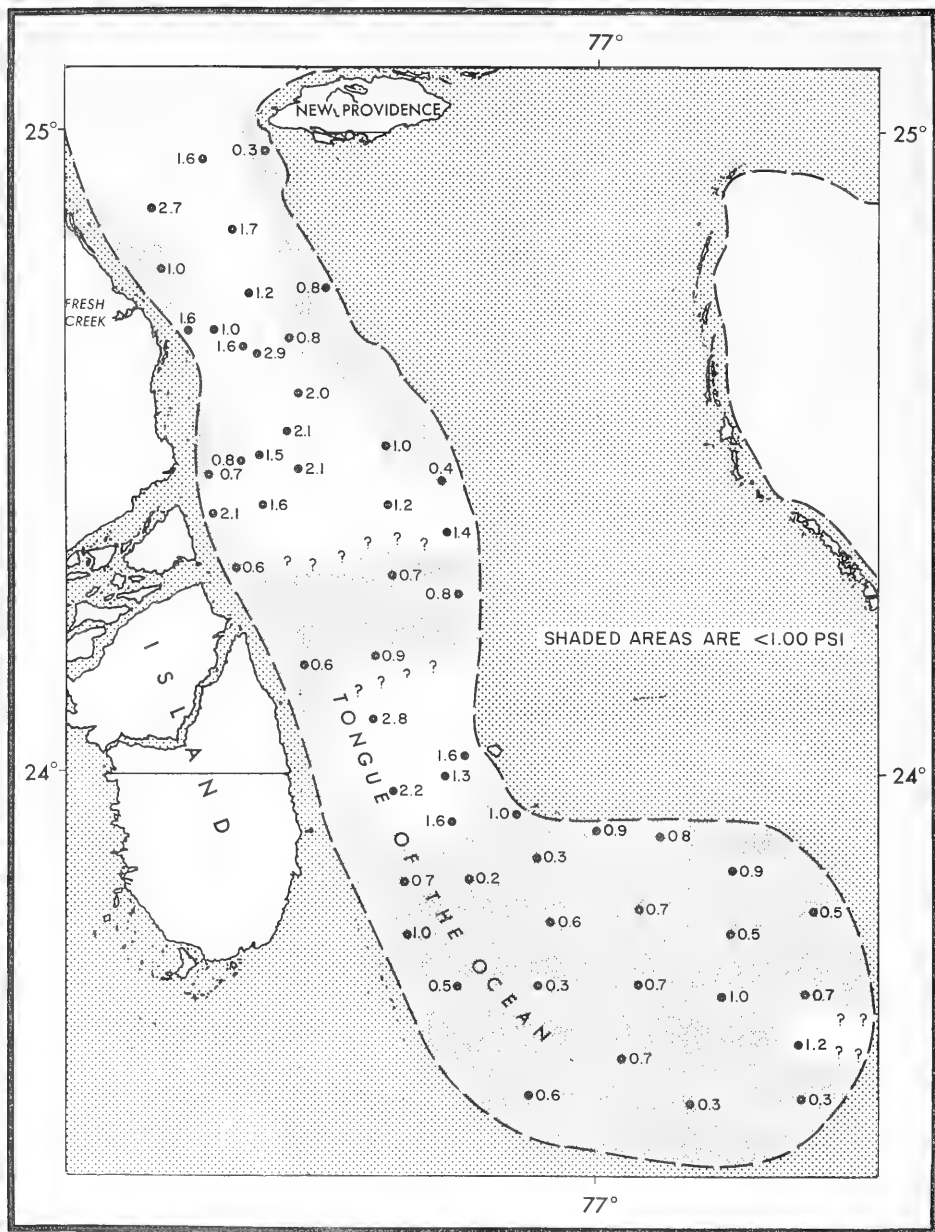


FIGURE 12 AREAS OF HIGH (>1.0 PSI) AND LOW COHESION IN THE TOTO

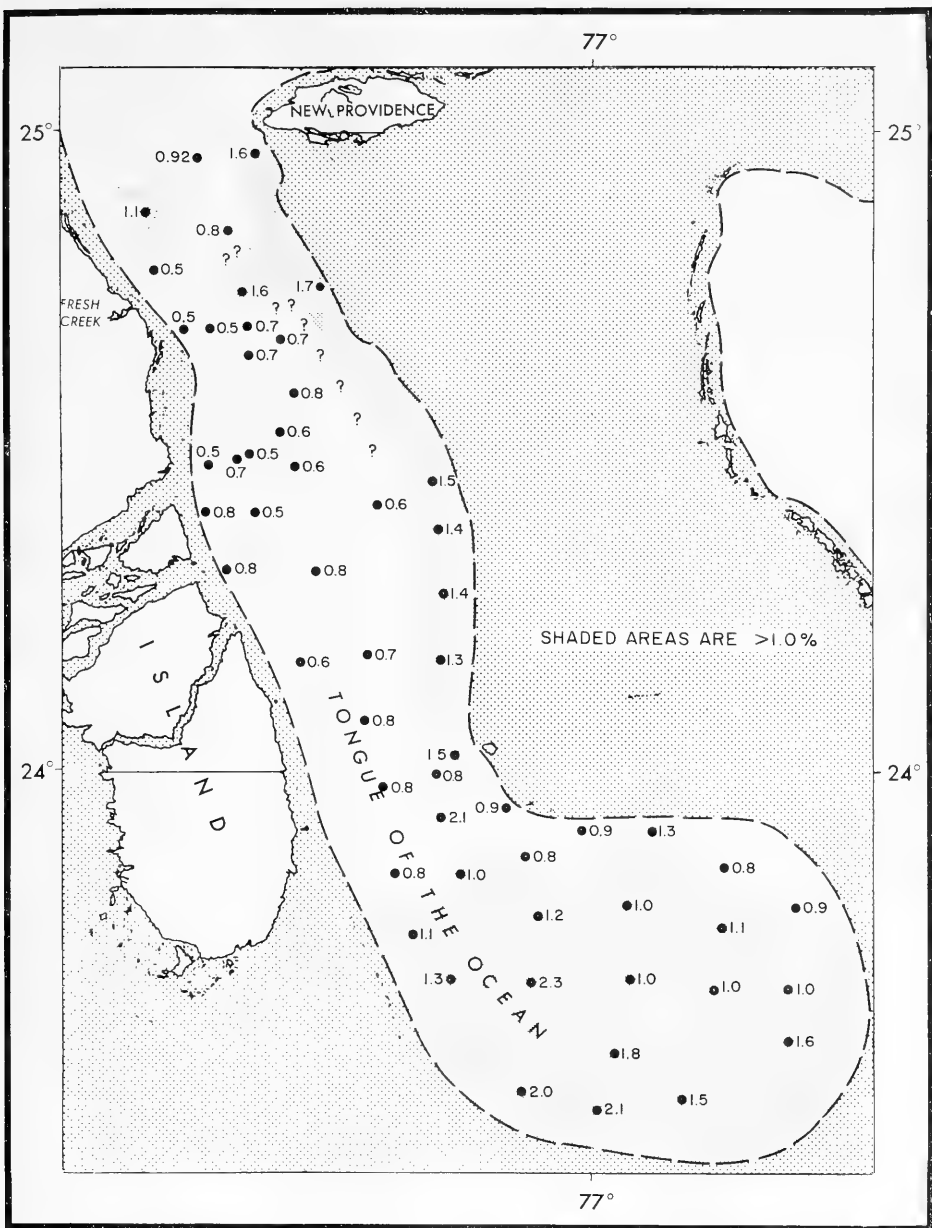


FIGURE 13 DISTRIBUTION OF SURFACE SEDIMENT ORGANIC CARBON CONTENT (%)

TABLE VII

Shear strength and sensitivity of the TOTO sediments

Core No.	Depth in Core (cm)	Shear Strength (psi)	Sensitivity
<u>Near-flank Sediments</u>			
61-1	3	1.0	
61-9	5	0.3	
	15	1.0	5
	48	1.5	
61-10	5	1.1	
	25	1.1	8
61-18	5	0.1	
	45	0.6	
	55	0.7	4
62-2	8	0.2	
	47	0.2	4
	94	0.6	
62-10	14	0.5	
	73	1.0	5
	138	0.9	
62-15	15	1.7	
	75	2.0	6
	121	2.6	
62-19	11	0.4	
	72	0.4	6
	118	0.5	
62-20	31	2.5	
	79	1.0	5
	130	0.7	
62-21	18	0.8	
	78	0.4	5
	136	1.1	
62-24	3	0.7	
	28	0.4	
	52	0.8	6
62-28	13	2.5	
	70	1.2	4
	142	1.2	

TABLE VII

Shear strength and sensitivity of the TOTO sediments (Cont'd)

Core No.	Depth in Core (cm)	Shear Strength (psi)	Sensitivity
<u>Near-flank Sediments (Cont'd)</u>			
62-37	3	0.1	
	59	1.6	2
62-39	11	0.3	
	48	1.3	2
	90	0.4	
62-57	10	0.2	
	74	1.8	2
	145	1.1	
62-58	3	0.1	
	46	0.3	2
	91	0.6	
<u>Axial Sediments</u>			
61-2	15	1.7	6
61-4	5	0.8	
	15	1.2	
	25	1.1	11
61-6	5	0.5	
	25	0.8	
	35	0.9	7
61-7	5	0.9	
	25	1.0	3
61-8	5	0.4	
	25	0.7	8
	45	1.6	
61-21	3	0.3	
	21	0.7	
	48	0.5	3
	76	1.0	
61-22B	11	2.9	7
62-2	27	1.0	
	84	0.7	7
	136	2.9	

TABLE VII

Shear strength and sensitivity of the TOTO sediments (Cont'd)

Core No.	Depth in Core (cm)	Shear Strength (psi)	Sensitivity
<u>Axial Sediments (Cont'd)</u>			
62-3	20	1.0	6
	65	3.1	
	120	2.9	
62-7	44	1.2	10
	88	1.8	
	147	1.8	
62-8	14	1.9	4
	42	1.0	
	74	0.7	
62-16	3	0.3	15
	80	0.9	
	156	3.5	
62-17	28	1.0	12
	76	1.9	
	113	3.7	
62-18	3	0.5	6
	46	1.3	
	109	2.0	
62-22	3	0.5	9
	28	0.5	
	52	2.1	
62-27	16	1.0	14
	56	4.3	
	108	3.2	
62-29	38	1.3	4
	104	0.5	
	129	2.0	
62-30	11	0.3	5
	66	1.0	
	120	3.6	
62-31	10	1.1	14
	78	1.9	
	149	3.7	
62-34	10	0.4	5
	68	0.5	
	146	2.1	

TABLE VII

Shear strength and sensitivity of the TOTO sediments (Cont'd)

Core No.	Depth in Core (cm)	Shear Strength (psi)	Sensitivity
<u>Axial Sediments (Cont'd)</u>			
62-47	3	1.1	6
62-48B	3	0.4	8
	52	1.8	
	101	0.7	
62-49	3	1.6	
62-50C	3	0.2	7
	44	1.1	
62-51B	3	0.2	5
	25	1.0	
	56	3.3	
62-52A	3	0.2	11
	52	2.2	
	97	4.0	
62-53	3	0.2	6
	52	0.8	
	102	1.6	
<u>Northeast Providence Channel</u>			
62-60	16	1.6	6
	42	1.3	
	82	4.2	
62-61	3	0.8	6
	68	0.7	
	133	0.8	
62-62	9	1.3	8
	73	1.0	
	138	1.5	
62-63	5	0.3	4
	32	0.9	
<u>Cul-de-sac Sediments</u>			
61-11	5	0.2	4
	35	0.4	

TABLE VII

Shear strength and sensitivity of the TOTO sediments (Cont'd)

Core No.	Depth in Core (cm)	Shear Strength (psi)	Sensitivity
<u>Cul-de-sac Sediments (Cont'd)</u>			
61-12	5	0.3	
	25	0.4	
61-16	5	0.3	
	28	1.2	
	51	0.7	
62-40	26	0.8	
	129	0.5	2
62-41	3	0.1	
	75	0.5	2
62-42	3	0.1	
	79	0.3	2
	137	1.5	
62-43	11	0.6	
	50	0.8	3
62-44	8	0.8	
	67	0.7	6
	131	0.9	
62-45	31	1.4	
	63	0.7	4
	94	0.6	
62-46	26	2.2	
	57	0.8	5
62-54	19	0.4	
	59	1.0	5
62-55	3	0.2	
	58	0.8	
62-56	3	0.2	
	47	0.8	2
	66	1.7	
62-59	22	1.0	



## Sensitivity

Sensitivities of core samples are given in Table VII. The values range from 2 to 16 (slightly insensitive to slightly quick) and show a predominance of very sensitive sediments. The cul-de-sac sediments are the least sensitive, axial sediments the greatest, and near-flank sediments intermediate between the two but tending more toward sensitivities similar to the cul-de-sac.

## BOTTOM PHOTOGRAPHY

Camera stations were located throughout the channel at predetermined positions. Although the photographs from this study cannot be considered to be representative of the entire channel bottom, the close-spaced coverage obtained along the fairly extensive tracks provides excellent representation in the area photographed, and, from these photographs and the work of Armstrong (1953) and Athern (1962 b) a general idea of the microrelief can be obtained.

Camera lowerings at Stations 1, 2, and 3 were occupied while the ship was at anchor, and the lowering at Station 4 was made while drifting. The ship's position was plotted and annotated during the camera lowerings on a Decca Hi-Fix plotter, and a graphic record of the ship's position, hence, the camera location ( $\pm 10$  feet), was obtained during the two-hour period while the camera was in operation off the bottom (Fig 14).

Camera lowering Station 4 is represented on Figure 14 by a line trending north-northwest across the center of the TOTO off High Cay. The paths followed by the other camera stations (1, 2, and 3) are also presented in this figure, and variations in ship location while at anchor are graphically demonstrated. In the graph of station 2, the ship completed one cycle of it's swing on the anchor cable, and the camera was brought up while halfway along the return swing.

The graph of Station 1 demonstrates the extreme to which the ship varied in position while anchored. In this instance, the vessel was subject to a fairly long-period pitch superimposed on the arc traversed around the anchoring point. The combination of swinging and surging produced a figure 8 pattern which the camera system followed. The procedure of plotting the ship movement, annotating the plot, and including a synchronized clock in the data chamber of the camera permits calculations to enable one to delete duplications of track coverage where present.

Two out of four of the camera stations produced pairs of stereo photographs (Stations 1 and 4), while at the remaining stations malfunctioning of one of the two cameras resulted in only one roll of exposures during the course of the lowering. The photographs generally cover an area approximately  $13.5' \times 8'$  or  $108 \text{ ft}^2$ , and overlapping of pairs exceeds one half the area photographed.

### Camera Station Data

Station 1

Depth: 1,250 meters

Number of Exposures: 362

Length of Camera Track: 457 meters

Track Position:  $23^{\circ} 27.4' \text{N}$ ,  $76^{\circ} 58.8' \text{W}$  (Coordinates for center of track)

Camera Performance: Stereographic pairs obtained from all exposures.

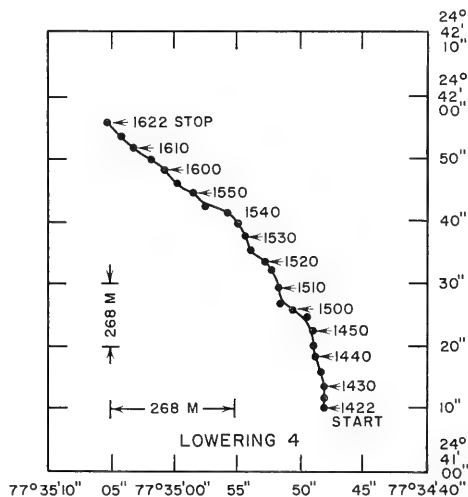
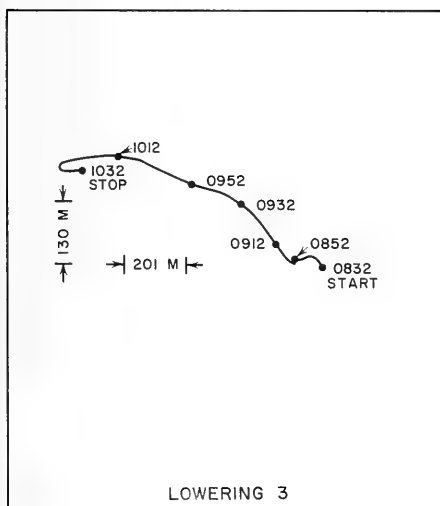
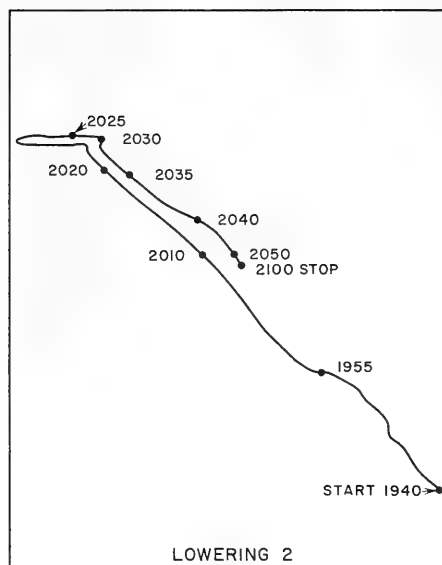
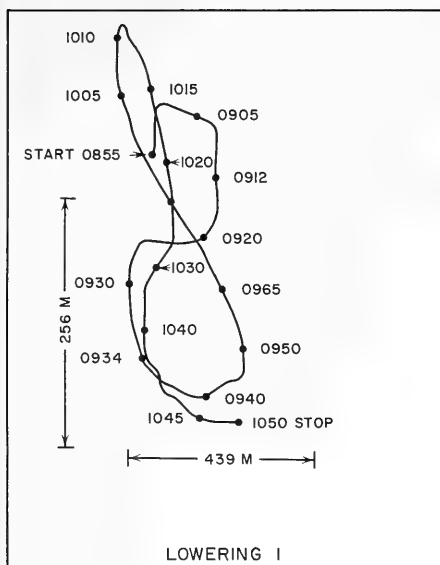


FIGURE 14 PLOT OF SHIP'S POSITION DURING CAMERA LOWERINGS

#### Station 2

Depth: 1,390 meters

Number of Exposures: 438

Length of Camera Track: 462 meters

Track Position: 24° 00'N, 77° 15.9'W (Coordinates for center of track)

Camera Performance: Right camera malfunctioned.

#### Station 3

Depth: 1,500 meters

Number of Exposures: 276

Length of Camera Track: 512 meters

Track Position: 24° 27.5'N, 77° 31.5'W (Coordinates for center of track)

Camera Performance: Left camera malfunctioned. Right camera produced 90 percent double exposures. Doubly exposed frames were, nevertheless, adequate for interpretation, and the good exposures obtained appear representative of the camera track.

#### Station 4

Depth: 1,929 meters

Number of Exposures: 572

Length of Camera Track: 1,572 meters

Track Position: 24° 41.6'N, 77° 34.8'W (Coordinates at start of track)

Camera Performance: Stereographic pairs obtained from all exposures.

### Biology

Animal life and evidence of its existence is extremely sparse along the tracks traversed by the camera system, and at only one site (Station 2) was there appreciable evidence, both direct and indirect, of a significant benthic population.

The majority of photographs obtained from all lowerings are devoid of animal life. A few holothurians were present to some degree in all the camera tracks (Plates III and VI), and occasional brittle stars (Plate III) were observable. Filamentous plant debris (probably derived from the shallow surrounding banks) was present on all tracks (see Plate IV for an example).

Stations 1 and 2 (Plates III and V) show the greatest direct and indirect evidence of organic activity, while, on the other hand, Stations 3 and 4 (Plates VI and VII) show no more than a featureless, unconsolidated calcareous ooze throughout the majority of the track.

Relative to the other camera tracks, Station 2 shows the most evidence of organic activity. Throughout the entire length of the track the bottom is thoroughly pitted and marked by trails, tracks, mounds, and burrows. A number of the mounds present in this and the remaining plates are thought to represent pebble and cobble debris which has been covered by sediment. These mounds are differentiated from organically derived mounds by the lack of an axial hole. Some sessile forms are present in the exposures from Station 2 which are suggestive of hydroids.

Armstrong (1953) reported that a very slow rate of sediment deposition prevails in the center of the TOTO, and any features on the bottom would tend to be preserved for a long time. If this is true then a small benthic population could produce bottom features which could be mistaken for a substantial benthic community. In any event, the information from the photographs point to an extreme paucity of bottom dwelling organisms on the floor of the TOTO. The low organic carbon values (consequently insufficient nutrients) obtained from analysis of the sediments substantiates these findings.

#### Bottom Features

Relief not connected with animal activity or particle-by-particle deposition over pre-existing features is present to a limited degree in specific areas along two of the camera tracks.

Photographs from Stations 2 and 3 showed no unexpected evidence of past or present constructional processes for the depth and position of the lowering, and, on the basis of the photographs, it is inferred that limited benthic faunal activity combined with a slow rate of sediment accumulation constitutes the dominant microrelief building processes.

Station 1, in the cul-de-sac, shows an outcrop of either a well lithified calcareous material covered by a sedimentary veneer or a semilithified bottom material (Plate IV). The outcrop strikes northeast, is of undeterminable thickness, and occurs on only two exposures (the closest points to the flank of the cul-de-sac) along the entire track. A slab of the outcropping material is observable in the top left photograph of Plate IV, and it appears to have moved, or is now moving, in a southerly direction. In the bottom two photographs on the same plate, circular pits or depressions a few centimeters in diameter and depth are apparent. The depressions show very steep sides and are located only in the photographs taken adjacent to the walls of the cul-de-sac. The dark material enclosed by a depression may represent pebble detritus washed off the adjacent banks; however, the apparent filamentous appearance of the material somewhat negates this possibility.

Camera lowering Station 4, although presenting the most featureless bottom for the first 1,500 meters of track, showed the most unexpected features of all the photographs. At 24° 41'49"N, 77° 35'01"W the camera system traversed a well indurated limestone outcrop approximately 24 feet across and terminating in a 3-foot vertical to concave scarp striking northeast (Plate VIII). Stereographic examination of the outcrop reveals cavities and depressions in the exposure which range from 5 to 60 centimeters in both width and depth, and, in many instances, unconsolidated sediment covers the base of the depression. A number of the cavities are interconnected to form a network of channels, and almost all display sharp angular rims (Plate IX). A microtopographic contour map of the edge of the outcrop is presented in Plate X.

Busby (1962) discussed this outcrop and the possible origin of the features, and concluded that the depressions are solution basins of subaerial or littoral zone origin that were formed when the outcrop or the floor of the channel was at an elevation of about 1,900 meters higher than at the present.

#### Bottom Currents

Twenty-four meters northwest of the outcrop observed in the photographs from Station 4, pebble and cobble-sized debris is present, and immediately adjacent to this material are well developed oscillatory ripple marks facing northeast (Plate XI). The ripple marks at this location appear symmetrical and average 13 centimeters from crest to crest.

Utilizing various sources of data, a rough estimate of the minimum current velocity necessary to produce these ripples can be calculated. The average median diameter of the surface sediments in the area of ripple mark formation is 15 microns, and, according to Hjulstrom (in Trask, 1955), a mean water velocity of 28 to 43 centimeters per second is required to instigate movement of particles of this diameter. Ripple marks disappear or are obliterated when water velocity exceeds a critical value, which in the instance of very coarse sands is 90 centimeters per second (Shipek, 1961). Consequently, a current of minimum velocity of 28 to 43 centimeters per second and maximum velocity of 90 centimeters per second is necessary for formation and maintenance of the ripple marks observed in Plate XI. The maximum velocity is probably much higher than that necessary to obliterate the ripples observed in this area; however, as no data are available concerning ripple marks in dominantly silt-sized sediments, this value is taken as the maximum in lieu of further information.

Menard (1952) attributed symmetrical ripple-mark development at 4,500 feet in the Pacific Ocean to short-period water oscillations perhaps caused by tides, tsunamis, or internal waves. Inman (1957) pointed out that symmetrical ripple marks require oscillatory currents for formation, since an unidirectional current produces asymmetrical ripples with one slope at the angle of repose of the sediment and the other more or less

concave. It is expected that at the depth (1,929 meters) of ripple occurrence in the TOTO, either internal waves or tidal oscillations produced the ripple marks observable, although the latter is more likely.

As mentioned above, adjacent to and south of the ripple-marked area is pebble- and cobble-sized debris which probably has been derived from the reef areas bounding the channel. From the photograph in Plate XI the ripple marks are apparent, and close study of the photograph shows the finer material to be encroaching upon the larger debris. The distribution of pebble and gravel material around the large cobble-sized fragment in the upper right-hand half of this photograph suggests a strong southerly current which is producing a lag deposit in this area with a net movement of sediment toward the south.

## SUMMARY

The significant results and conclusions from the bottom sediment investigations in the TOTO by this Office and previous investigations by others are summarized below:

1. The TOTO is a long, narrow channel in the Great Bahama Bank which gradually increases in depth from about 700 fathoms in the southern cul-de-sac area to 1,300 fathoms in the northern portion at the commencement of Northeast Providence Channel.

2. The flanks of the TOTO are steep (15 to 20°) bare rock walls to depths of 100 to 200 fathoms. Below this depth to the bottom of the channel the slope is more gentle, incised by gullies normal to the Bank edge and sediment covered.

3. The sediments on the floor of the channel are:

- a. Almost wholly composed of calcium carbonate,
- b. Dominantly silt-sized particles with a slight increase in sand in sediments collected from central reaches of the channels,
- c. Composed predominantly of the tests of planktonic foraminifera, pteropods, and reef detritus, and
- d. In general, poorly sorted.

4. A reducing environment prevails in the sediments on the flanks and, to a lesser degree in the cul-de-sac, while an oxidizing environment prevails in the sediments in the flat central reaches of the northern, elongated portion of the channel.

5. Sediment density is greatest in the axial region and lowest in the near-flank and cul-de-sac areas; conversely, water content, void ratio, and porosity are lowest in the axial region and highest in the near-flank and cul-de-sac areas.

6. Sediment density generally increases with depth in the sediment while water content, void ratio, and porosity decrease.

7. Over one-half of the sediment column sampled in the axial and cul-de-sac areas is the result of turbidity current deposition, while the near-flank sediments appear to be primarily the result of particle-by-particle accumulation from the overlying water column.



8. Turbidity currents originate on the upper flanks of the channel, flow down slope at high velocity within the gullies, and distribute the sediment load locally on the channel floor.

9. Frequency of the turbidity flows is greatest in the cul-de-sac area and becomes less frequent northward in the channel. Rate of sediment accumulation is highest on the channel flanks and becomes less northward from the cul-de-sac along the channel axis.

10. Ultimate bearing strength of the sediment is lowest in the cul-de-sac and near-flank areas, highest in the axial area, and can be shown to follow the same trend as the organic carbon and water content of the sediments.

11. Bottom photographs show a paucity of benthic fauna, and, in general, a relatively featureless, unconsolidated ooze covers the channel floor.

12. The photographs reveal a bare rock outcrop at 1,000 fathoms in the center of the channel off Fresh Creek. Features in the outcrop indicate subaerial erosion of the exposure at some earlier geologic time.

13. Ripple marks present in some of the bottom photograph suggest a bottom current at 1,000 fathoms of at least 0.3 to 0.7 knot.

## REFERENCES CITED

- Agassiz 1894 A reconnaissance of the Bahamas and of the elevated reefs of Cuba in the steam yacht "Wild Duck" January to April 1893. Bull. Mus. Comp. Zool., v. 26, no. 1, pp. 10203.
- Allison, L. E. 1935 Organic soil carbon by reduction of chromic acid. Soil Sci., v. 40, pp. 311-320.
- Armstrong, J. C. 1953 Oceanography of the Tongue of the Ocean, Bahamas, B. W. I. Office of Naval Research, Nonr-04501, 12 p.
- Athern, W. D. 1962 a Bathymetric and sediment survey of the Tongue of the Ocean, Bahamas, Part I: Bathymetry and sediments. Woods Hole Oceanog. Inst. Ref. No. 62-25, 17 pp.
- - 1962 b Bathymetric and sediment survey of the Tongue of the Ocean, Bahamas, Part II. Bottom photographs. Woods Hole Oceanog. Inst. Ref. No. 62-27, 3 pp., 26 pl.
- Busby, R. F. 1962 Subaerial features on the floor of the Tongue of the Ocean, Bahamas. NAVOCEANO IMR No. 0-48-62. Unpublished Manuscript.
- Drew, G. H. 1914 On the precipitation of calcium carbonate in the sea by marine bacteria, and on the action of denitrifying bacteria in tropical and temperate seas. Carnegie Inst. Washington, Pub. 182, v. 5, pp. 7-45.
- Eardley, A. J. 1951 Structural geology of North America. Harper & Bros., New York, p. 573.
- Ericson, D. B., M. Ewing, and B. Heezen 1952 Turbidity currents and sediments in North Atlantic. Bull. Amer. Assoc. Petrol. Geol., v. 36, pp. 489-511.
- - -, M. Ewing, G. Woolin, and B. Heezen 1961 Atlantic deep-sea sediment cores. Bull. Amer. Assoc. Petrol. Geol. v. 72, pp. 193-286.
- Field, R. M., and collaborators 1931 Geology of the Bahamas. Bull. Amer. Assoc. Petrol. Geol., v. 42, pp. 759-784.
- Goldmen, M. I. 1926 Proportions of detrital organic calcareous constituents and their chemical alteration in a reef sand from the Bahamas. Carnegie Inst. Washington Pub. 344, v. 23, pp. 39-65.

- Hess, H. H. 1933 Interpretations of geological and geophysical observations in Navy Princeton Gravity Expedition to the West Indies in 1932. U. S. Navy Hydrographic Office, Washington, D. C., pp. 27-53.
- Hjulstrom, F. 1955 Transportation of detritus by moving water. In recent Marine Sediments, a Symposium, Soc. Econ. Paleon. and Min., Special Pub. No. 4, Parker D. Trask, Editor, pp. 5-31.
- Illing, L. V. 1954 Bahaman calcareous sands. Bull. Amer. Assoc. Petrol. Geol. v. 38, pp. 1-95.
- Inman, D. L. 1957 Wave generated ripples in near shore sands, Dept. of the Army Technical Mem. No. 100, 41 pp.
- Kuenen, Ph. H. 1953 Significant features of graded bedding. Bull. Amer. Assoc. Petrol. Geol., v. 37, pp. 1044-1066.
- - -, and H. W. Menard 1952 Turbidity currents, graded and nongraded deposits. Jour. Sed. Pet., v. 22, 83-96.
- Marine Laboratory, University of Miami 1958 Oceanographic survey of the Tongue of the Ocean. Technical Report, 26 September 1958, v. 1.
- Menard, H. W. 1952 Deep ripple marks in the sea. Jour. Sed. Pet., v. 22, pp. 3-9.
- Nelson, R. J. 1853 On the geology of the Bahamas, and on coral-formations generally. Geol. Soc. London, Quart-Jour. v. 9, 200-215.
- Newell, N. D. 1955 Bahamian platforms. in: The Cruise of the Earth, A symposium, Geol. Soc. Amer., Special Paper 62, pp. 303-315.
- - -, J. K. Rigby, A. J. Whiteman, and J. S. Bradley 1951 Shoal Water geology and environments, eastern Andros Island, Bahamas, Bull. Amer. Mus. Nat. Hist., v. 97 00. 1-9.
- - -, and J. K. Rigby 1957 Geologic studies on the Great Bahama Bank; in: Regional Aspects of Carbonate Deposition, a Symposium with discussions, Soc. Econ. Paleon. Min., Special Pub. No. 5, pp. 15-79.
- Olausson, E. 1961 Studies of deep-sea cores. Reports of the Swedish Deep-Sea Expedition 1947-1948, v. 8, fasc. 4, pp. 335-391.

- Ostlund, H. G., A. L. Bowman, and G. A. Rusnak 1962 Miami natural radio-carbon measurements. *Radiocarbon*, v. 4, pp. 51-56.
- Richards, A. F. 1961 Investigations of deep-sea sediment cores. I. Shear strength, bearing capacity, and consolidation. U. S. Navy Hydrographic Office, Washington, D. C., Technical Report 63, 70 pp.
- Revelle, R. R. 1944 Marine bottom samples collected in the Pacific Ocean by the Carnegie on its seventh cruise. Carnegie Inst. of Washington Pub. 556, pp. 1-183.
- Rusnak, G. A., and W. D. Nesteroff 1962 Modern turbidites: terrigenous abyssal plain versus bioclastic basin. Contrib. No. 000, the Marine Lab. Univ. of Miami, (In Press).
- Schuchert, C. 1934 Historical geology of North America, v. I. Antillean-Caribbean region. John Wiley & Sons, New York, 811 pp.
- Shipek, C. J. 1961 Microrelief on the sea floor. *Sci. Teacher*, v. 28, 7 pp.
- Siegler, V. B. 1961 Bathymetric reconnaissance of Exuma Sound. The Marine Laboratory, Univ. of Miami Technical Report 61-4, 9 pp.
- Talwani, M., J. L. Worzel, and M. Ewing 1959 Gravity anomalies and structure of the Bahamas. *Lamont Geol. Obs., Columbia Univ., New York, Unpubl. Ms.*, pp. 1-9.
- Terzaghi, K., and R. B. Peck 1948 Soil mechanics in engineering practice. John Wiley & Sons, Inc., New York, 566 pp.
- Thorp, E. M. 1936 Calcareous shallow-water marine deposits of Florida and the Bahamas. Carnegie Inst. Washington Pub. 452, pp. 37-143.
- Turkian, K. K. 1956 Rapid technique for determination of carbonate content of deep-sea cores. *Bull. Amer. Assoc. Petrol. Geol.*, v. 40, pp. 2507-2509.
- Vasicek, M. 1953 Graded bedding and some sedimentary mineral deposits: Sborník Ustředního Ústavu Geologického, Svazek XX, Nakladatelství Československé Akademie, Praha, 52 pp.
- Vaughan, T. W. 1913 Remarks on the geology of the Bahamas Islands, and on the formation of the Floridian and Bahamian oolites. *Jour. Washington Acad. Sci.*, v. 3, n. 10, pp. 302-304.

- Vaughan, T. W. 1914 Preliminary remarks on the geology of the Bahamas, with special reference to the origin of the Bahaman and Floridian oolites. Carnegie Inst. Washington Pub. 182, v. 5, pp. 47-54.
- - - 1918 Some shoal-water bottom samples from Murray Island, Australia, and comparisons of them with samples from Florida and the Bahamas. Carnegie Inst. Washington Pub. 213, v. 9, pp. 239-288.
- Wentworth, C. K. 1922 A scale of grade and class terms for clastic sediments. Jour. Geol., v. 30, pp. 377-392.
- Woodring, W. P. 1928 Tectonic features of the Caribbean region. Third Pan-Pacific Sci. Congr. Tokyo, 1926, Proc., pp. 401-432.
- Worzel, J. L., M. Ewing, and C. L. Drake 1953 Gravity observations at sea, Pt. I, the Bahama Islands region. Bull. Geol. Soc. Amer., v. 64, pp. 1494-1495 (abstract).



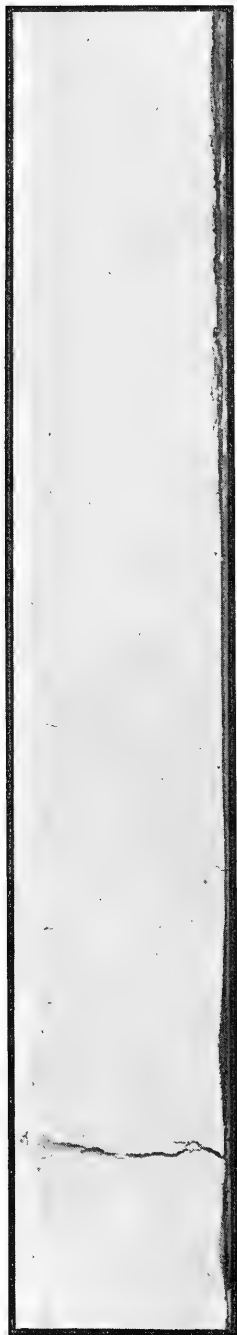
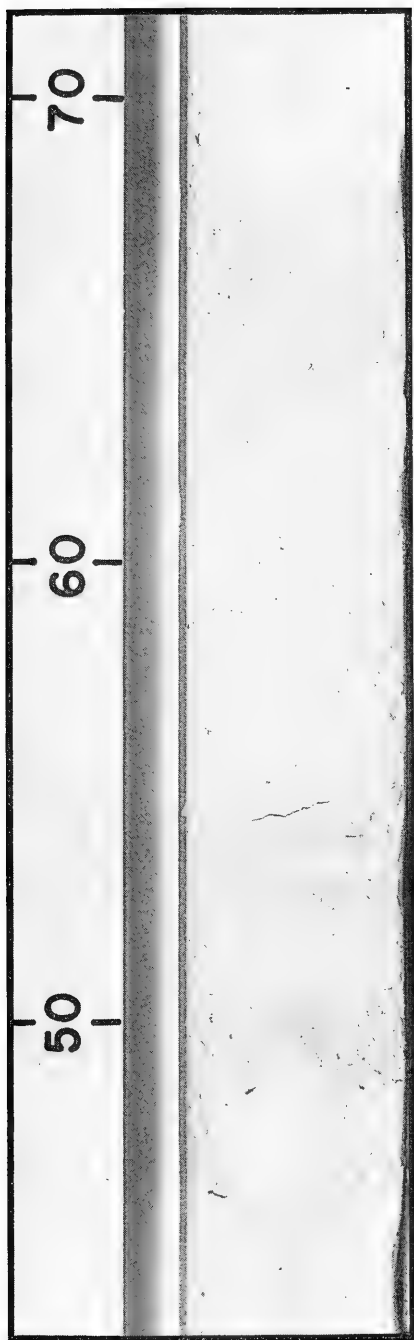


PLATE 1 AXIAL CORE 62-16 (TOP) AND NEAR-FLANK CORE 62-15 (BOTTOM). NOTE LIGHTER HUE, COLOR BANDS, AND ROUGH TEXTURE OF THE AXIAL CORE AS OPPOSED TO THE SMOOTH, EVEN TEXTURE AND COLOR OF THE NEAR-FLANK CORE. SCALE IN CENTIMETERS.

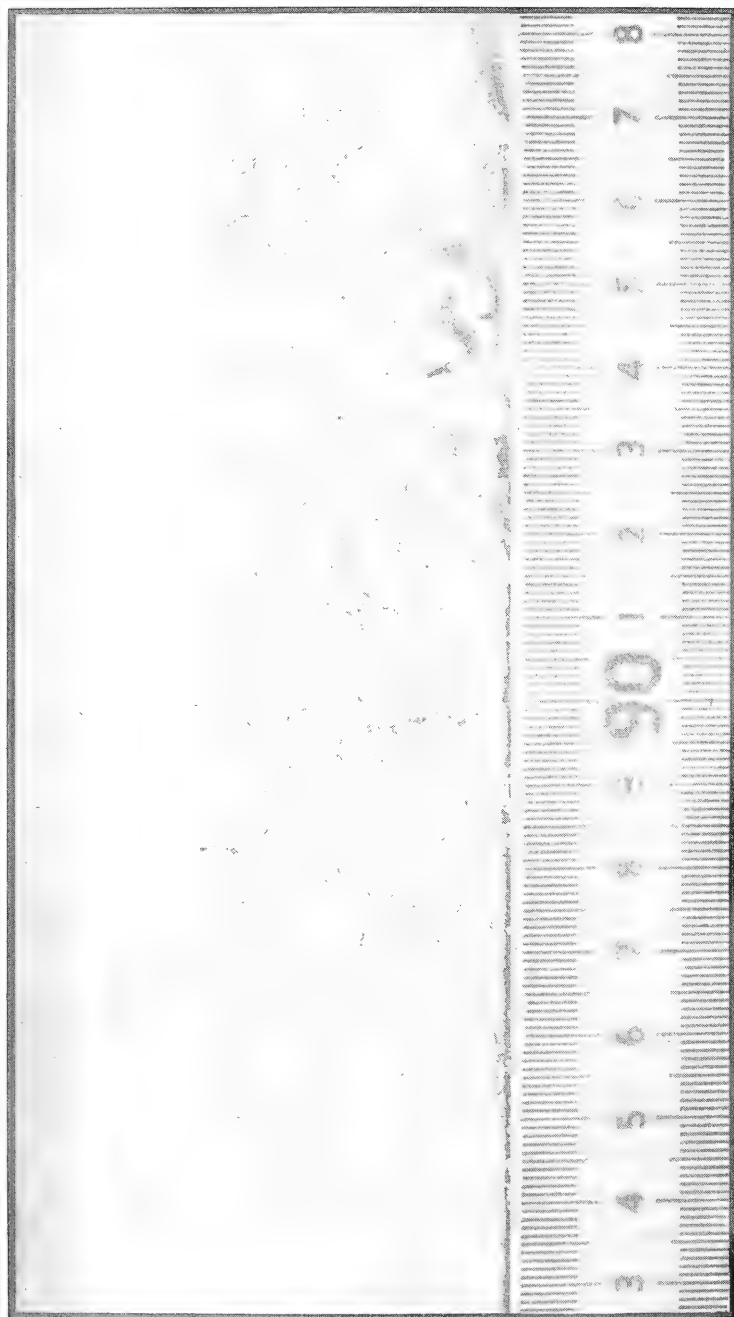


PLATE II TURBIDITE ZONE IN CORE 62-48B. NOTE GRADATION IN PARTICLE SIZE FROM COARSE TO FINE UPWARD IN THE CORE (RIGHT TO LEFT). NEEDLE-LIKE PARTICLES AT 93 CENTIMETERS ARE PTEROPODS OF THE GENUS CRESEIS. SCALE IN CENTIMETERS.





PLATE III REPRESENTATIVE BOTTOM PHOTOGRAPHS FROM CAMERA STATION 1. NOTE HOLOTHURIANS AND THEIR TRACKS IN LOWER LEFT PHOTOGRAPH, AND BRITTLE STAR JUST ABOVE CENTER IN TOP LEFT PHOTOGRAPH. THE RADIAL ARRANGEMENTS PRESENT THROUGHOUT ALL THE PHOTOGRAPHS ARE BELIEVED TO REPRESENT A SEARCH PATTERN BY SOME TYPE ANNELID.

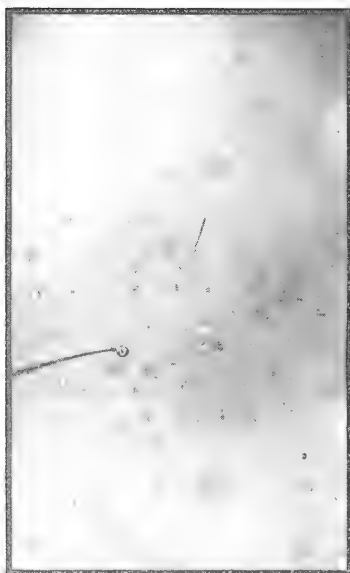


PLATE IV BOTTOM PHOTOGRAPHS FROM CAMERA STATION 1. NOTE OUTCROP IN TOP RIGHT PHOTOGRAPH AND BOULDER IN TOP LEFT. LOWER TWO PHOTOGRAPHS SHOW CIRCULAR PITS OR DEPRESSIONS AND SCATTERED PLANT DETRITUS.

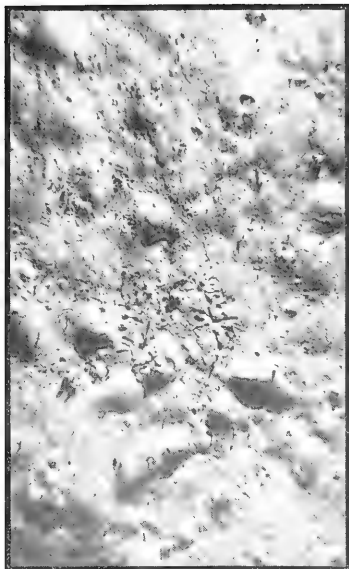


PLATE V REPRESENTATIVE BOTTOM PHOTOGRAPHS FROM CAMERA STATION 2.

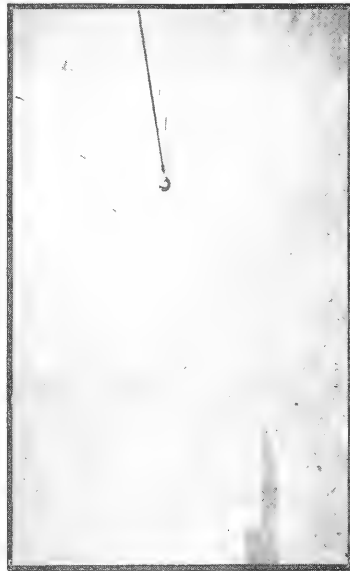
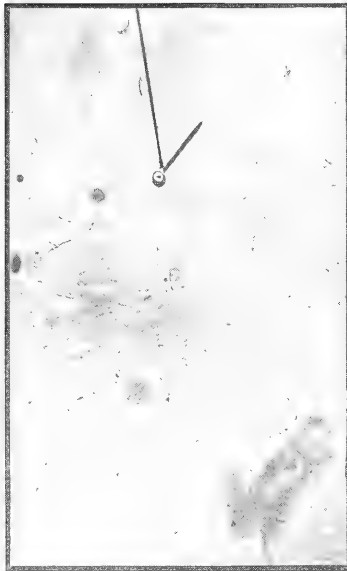


PLATE VI REPRESENTATIVE BOTTOM PHOTOGRAPHS FROM CAMERA STATION 3.

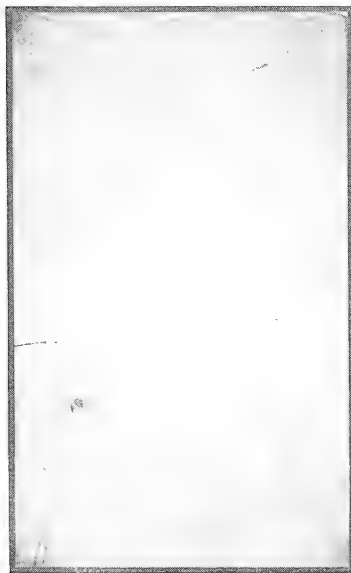


PLATE VII REPRESENTATIVE BOTTOM PHOTOGRAPHS FROM CAMERA STATION 4.  
NOTE CRUSTACEAN IN BOTTOM RIGHT PHOTOGRAPH.

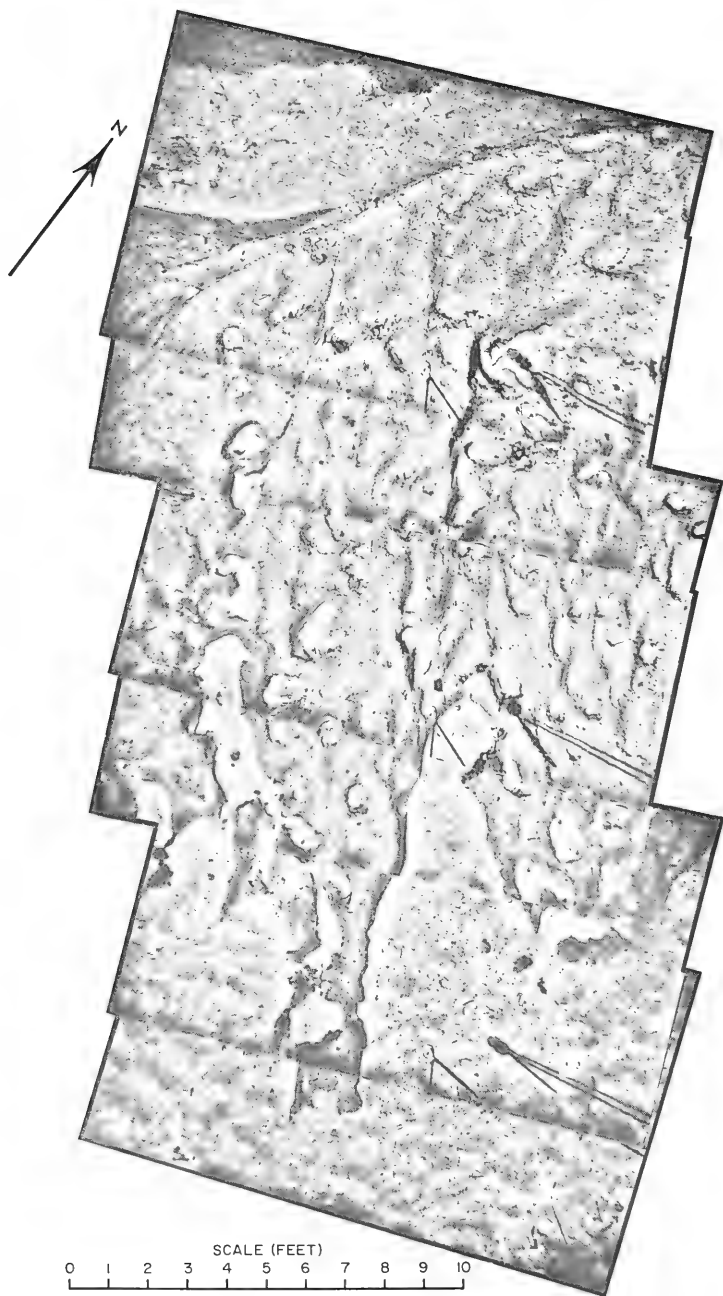
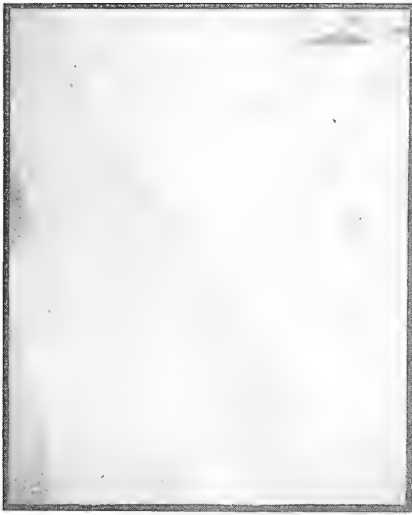
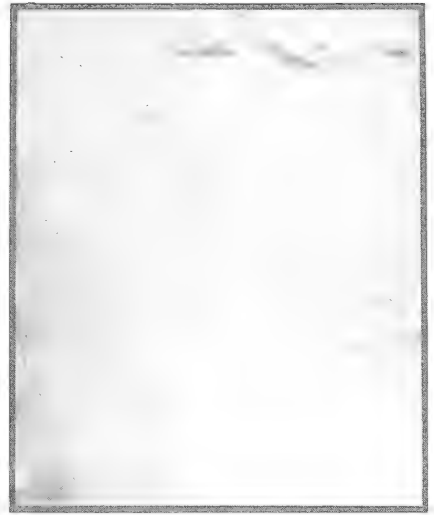


PLATE VIII MOSAIC OF THE OUTCROP AS PHOTOGRAPHED BY THE CAMERA SYSTEM



A



SCALE 1:34



B

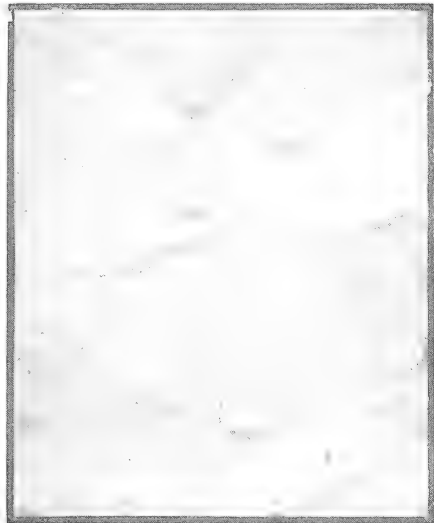


PLATE 1X CAVITIES AND DEPRESSIONS AT 1,000 FATHOMS IN THE TONGUE OF THE OCEAN. THE SCARP PRESENT IN THE UPPER PHOTOGRAPH IS APPROXIMATELY 3 FEET DEEP.

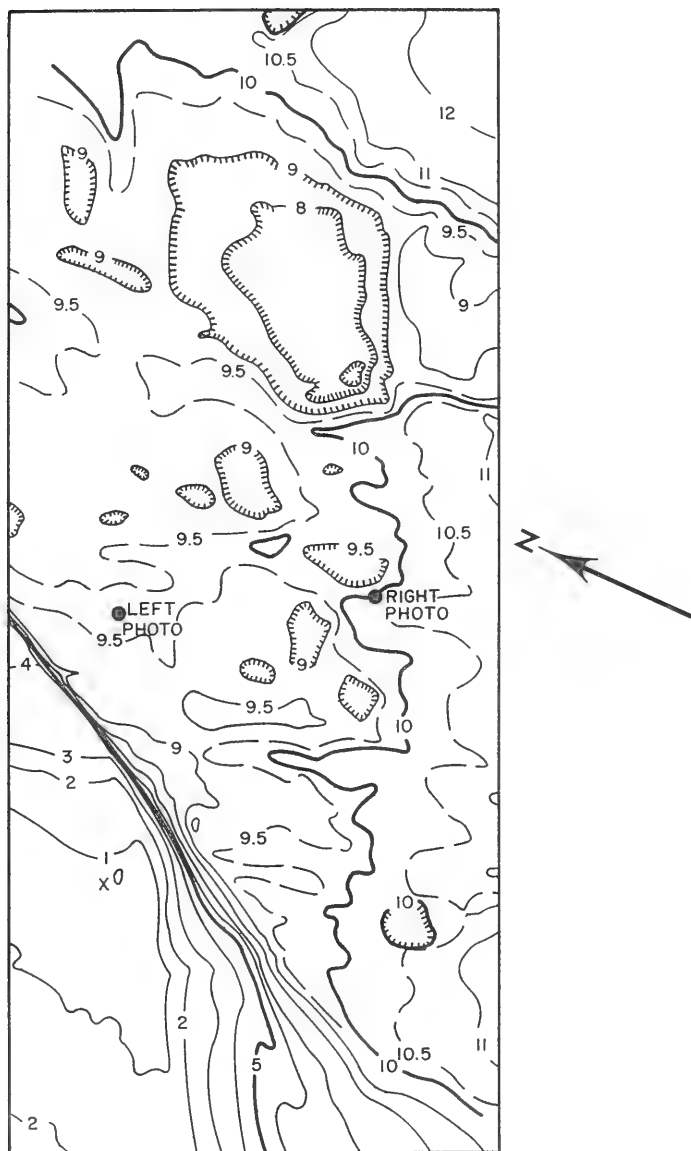


PLATE X MICROTOPOGRAPHIC CONTOUR MAP OF PLATE IX  
CONTOUR INTERVAL: 1 DECIMETER, SCALE: 1:17.8



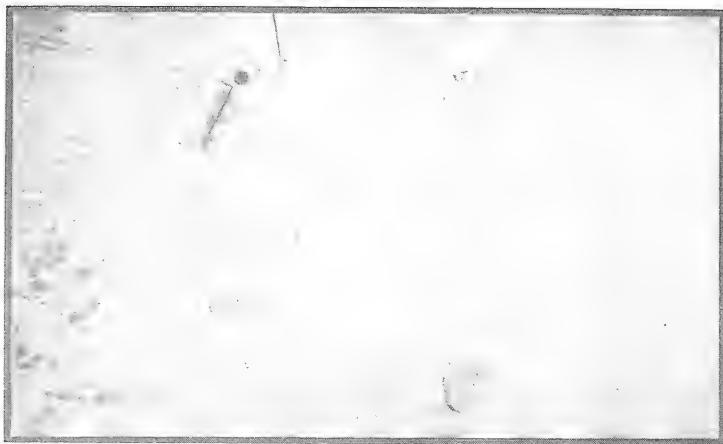


PLATE XI BOTTOM PHOTOGRAPHS FROM CAMERA STATION 4. OBSERVE THE STREAMING OF FINER FRAGMENTS SOUTHWARD OF THE LARGE COBBLE ON THE LOWER PORTION OF THE TOP PHOTOGRAPH; ALSO, THE SMOOTHER, MORE PLANATED APPEARANCE OF THE RIPPLE MARKS TO THE RIGHT OF THIS PHOTOGRAPH AS OPPOSED TO THE RIPPLES ON THE BOTTOM PHOTOGRAPH. SCALE APPROXIMATELY 1:34.



# APPENDIX I CORE STATION DATA

Core No.	Latitude (N)	Longitude (W)	Depth (m)	Length of Core (cm)
62-1	24° 58.2'	77° 39.3'	677	100
62-2	24° 57'	77° 40'	1829	151
62-3	24° 55.2'	77° 45.8'	1840	127
62-4	24° 51.9'	77° 50'	558	Grab Sample
62-5	24° 43'	77° 43'	580	13
62-6	24° 40'	77° 41'	498	Grab Sample
62-7	24° 40.1'	77° 36.1'	1710	158
62-8	24° 44.1'	77° 36.1'	1889	81
62-9	24° 49.2'	77° 30.3'	841	31
62-10	24° 45'	77° 28'	950	147
62-11	24° 41.2'	77° 25.1'	988	Grab Sample
62-13	24° 35'	77° 30'	1683	153
62-14	24° 35'	77° 39.9'	640	27
62-15	24° 24'	77° 39.9'	457	129
62-16	24° 24.2'	77° 34.7'	1480	175
62-17	24° 28'	77° 30'	1868	121
62-18	24° 24.6'	77° 22.4'	1202	121
62-19	24° 27'	77° 15.9'	1051	127
62-20	24° 22'	77° 15'	525	140
62-21	24° 16.1'	77° 14.9'	1041	148
62-22	24° 17.1'	77° 22.2'	1463	88
62-23	24° 17.9'	77° 28.1'	1481	40
62-24	24° 19'	77° 37.2'	768	59
62-25	24° 14.2'	77° 34.4'	430	13
62-26	24° 03'	77° 29'	612	Grab Sample
62-27	24° 04.6'	77° 23.2'	1399	116
62-28	24° 01.1'	77° 14.2'	1728	152
62-29	23° 58.9'	77° 16.1'	1353	136
62-30	23° 55.2'	77° 15.1'	1344	126
62-31	23° 57.7'	77° 21.1'	1362	159
62-32	23° 57.9'	77° 27'	805	12
62-33	23° 53.2'	77° 25.2'	823	Grab Sample
62-34	23° 44.7'	77° 19'	1134	157
62-35	23° 39'	77° 16'	1234	Grab Sample
62-36	23° 34'	77° 12'	1243	72
62-37	23° 28.9'	77° 06.7'	1066	63
62-38	23° 27'	76° 59.3'	1179	48
62-39	23° 28'	76° 51'	1253	97

# APPENDIX I CORE STATION DATA (Cont'd)

Core No.	Latitude (N)	Longitude (W)	Depth (m)	Length of Core (cm)
62-40	23° 33'	76° 57'	1326	138
62-41	23° 39.5'	77° 05.9'	1330	149
62-42	23° 46'	77° 05'	1330	146
62-43	23° 47'	76° 55.8'	1134	106
62-44	23° 53.8'	76° 53.3'	1244	137
62-45	23° 55.1'	77° 00'	1253	101
62-46	23° 56'	77° 09.7'	1198	98
62-47	24° 41'	77° 35'	1810	21
62-48	24° 41.3'	77° 39'	1300	113
62-49	24° 41.3'	77° 42'	811	16
62-50	24° 28.5'	77° 39'	1609	53
62-51	24° 30'	77° 34.9'	1573	66
62-52A	24° 31.6'	77° 32'	1640	107
62-53	23° 50.8'	76° 45.8'	1250	109
62-54	23° 45.1'	76° 46.2'	1293	68
62-55	23° 47'	76° 38.3'	1262	130
62-56	23° 39.4'	76° 39.5'	1234	72
62-57	23° 34'	76° 39'	1174	151
62-58	23° 29.1'	76° 39'	871	93
62-59	23° 39.5'	76° 47'	1282	66
62-60	25° 42'	77° 47'	1701	89
62-61	25° 19'	77° 59.5'	1300	141
62-62	25° 13.8'	77° 35.8'	2800	144
62-63	25° 41'	77° 34'	1728	42
61-1	24° 46.6'	77° 44.6'	1225	69
61-2	24° 49.7'	77° 37.3'	1875	30
61-4	24° 30'	77° 21.9'	1280	34
61-6	24° 29.6'	77° 36'	1590	46
61-7	24° 10.3'	77° 29.6'	1161	46
61-8	24° 10.5'	77° 22.7'	1481	69
61-9	24° 09.3'	77° 15.1'	934	71
61-10	23° 49.7'	77° 19.8'	1170	51
61-11	23° 49.7'	77° 13'	1414	65
61-12	23° 51.8'	77° 06.2'	1390	53
61-16	23° 39.5'	76° 55.6'	1314	57
61-18	23° 39.7'	77° 14.3'	1202	87
61-21	24° 40.5'	77° 30.5'	1500	98
61-22	24° 39'	77° 35'	1774	32

U. S. Naval Oceanographic Office  
SUBMARINE GEOLOGY OF THE TONGUE  
OF THE OCEAN, BAHAMAS, by Roswell F.  
Busby, November 1962. 84 p., 14 figs., 11  
plates, 1 app. (TR-108).

References p. 66 to 69

This publication presents a comprehensive  
report on the submarine geology of the Tongue  
of the Ocean, Bahamas. Material is based on  
both published and unpublished sources of  
information.

1. Submarine Geology - Tongue of  
the Ocean
2. Tongue of the Ocean - Submarine  
Geology
3. Oceanography - Tongue of the  
Ocean
4. Tongue of the Ocean - Oceanography
- i. title: Submarine Geology of the  
Tongue of the Ocean, Bahamas
- ii. author: Roswell F. Busby
- iii. TR-108

U. S. Naval Oceanographic Office  
SUBMARINE GEOLOGY OF THE TONGUE  
OF THE OCEAN, BAHAMAS, by Roswell F.  
Busby, November 1962. 84 p., 14 figs., 11  
plates, 1 app. (TR-108).

References p. 66 to 69

This publication presents a comprehensive  
report on the submarine geology of the Tongue  
of the Ocean, Bahamas. Material is based on  
both published and unpublished sources of  
information.

1. Submarine Geology - Tongue of  
the Ocean
2. Tongue of the Ocean - Submarine  
Geology
3. Oceanography - Tongue of the  
Ocean
4. Tongue of the Ocean - Oceanography
- i. title: Submarine Geology of the  
Tongue of the Ocean, Bahamas
- ii. author: Roswell F. Busby
- iii. TR-108

U. S. Naval Oceanographic Office  
SUBMARINE GEOLOGY OF THE TONGUE  
OF THE OCEAN, BAHAMAS, by Roswell F.  
Busby, November 1962. 84 p., 14 figs., 11  
plates, 1 app. (TR-108).

References p. 66 to 69

This publication presents a comprehensive  
report on the submarine geology of the Tongue  
of the Ocean, Bahamas. Material is based on  
both published and unpublished sources of  
information.

1. Submarine Geology - Tongue of  
the Ocean
2. Tongue of the Ocean - Submarine  
Geology
3. Oceanography - Tongue of the  
Ocean
4. Tongue of the Ocean - Oceanography
- i. title: Submarine Geology of the  
Tongue of the Ocean, Bahamas
- ii. author: Roswell F. Busby
- iii. TR-108

U. S. Naval Oceanographic Office  
SUBMARINE GEOLOGY OF THE TONGUE  
OF THE OCEAN, BAHAMAS, by Roswell F.  
Busby, November 1962. 84 p., 14 figs., 11  
plates, 1 app. (TR-108).

References p. 66 to 69

This publication presents a comprehensive  
report on the submarine geology of the Tongue  
of the Ocean, Bahamas. Material is based on  
both published and unpublished sources of  
information.

1. Submarine Geology - Tongue of  
the Ocean
2. Tongue of the Ocean - Submarine  
Geology
3. Oceanography - Tongue of the  
Ocean
4. Tongue of the Ocean - Oceanography
- i. title: Submarine Geology of the  
Tongue of the Ocean, Bahamas
- ii. author: Roswell F. Busby
- iii. TR-108



U. S. Naval Oceanographic Office  
SUBMARINE GEOLOGY OF THE TONGUE  
OF THE OCEAN, BAHAMAS, by Roswell F.  
Busby, November 1962. 84 p., 14 figs., 11  
plates, 1 app. (TR-108).

References p. 66 to 69

This publication presents a comprehensive  
report on the submarine geology of the Tongue  
of the Ocean, Bahamas. Material is based on  
both published and unpublished sources of  
information.

1. Submarine Geology - Tongue of  
the Ocean
2. Tongue of the Ocean - Submarine  
Geology
3. Oceanography - Tongue of the  
Ocean
4. Tongue of the Ocean - Oceanography
- i. title: Submarine Geology of the  
Tongue of the Ocean, Bahamas
- ii. author: Roswell F. Busby
- iii. TR-108

U. S. Naval Oceanographic Office  
SUBMARINE GEOLOGY OF THE TONGUE  
OF THE OCEAN, BAHAMAS, by Roswell F.  
Busby, November 1962. 84 p., 14 figs., 11  
plates, 1 app. (TR-108).

References p. 66 to 69

This publication presents a comprehensive  
report on the submarine geology of the Tongue  
of the Ocean, Bahamas. Material is based on  
both published and unpublished sources of  
information.

1. Submarine Geology - Tongue of  
the Ocean
2. Tongue of the Ocean - Submarine  
Geology
3. Oceanography - Tongue of the  
Ocean
4. Tongue of the Ocean - Oceanography
- i. title: Submarine Geology of the  
Tongue of the Ocean, Bahamas
- ii. author: Roswell F. Busby
- iii. TR-108

U. S. Naval Oceanographic Office  
SUBMARINE GEOLOGY OF THE TONGUE  
OF THE OCEAN, BAHAMAS, by Roswell F.  
Busby, November 1962. 84 p., 14 figs., 11  
plates, 1 app. (TR-108).

References p. 66 to 69

This publication presents a comprehensive  
report on the submarine geology of the Tongue  
of the Ocean, Bahamas. Material is based on  
both published and unpublished sources of  
information.

1. Submarine Geology - Tongue of  
the Ocean
2. Tongue of the Ocean - Submarine  
Geology
3. Oceanography - Tongue of the  
Ocean
4. Tongue of the Ocean - Oceanography
- i. title: Submarine Geology of the  
Tongue of the Ocean, Bahamas
- ii. author: Roswell F. Busby
- iii. TR-108

U. S. Naval Oceanographic Office  
SUBMARINE GEOLOGY OF THE TONGUE  
OF THE OCEAN, BAHAMAS, by Roswell F.  
Busby, November 1962. 84 p., 14 figs., 11  
plates, 1 app. (TR-108).

References p. 66 to 69

This publication presents a comprehensive  
report on the submarine geology of the Tongue  
of the Ocean, Bahamas. Material is based on  
both published and unpublished sources of  
information.

1. Submarine Geology - Tongue of  
the Ocean
2. Tongue of the Ocean - Submarine  
Geology
3. Oceanography - Tongue of the  
Ocean
4. Tongue of the Ocean - Oceanography
- i. title: Submarine Geology of the  
Tongue of the Ocean, Bahamas
- ii. author: Roswell F. Busby
- iii. TR-108







